NASA TN D-1767

TECHNICAL NOTE
D-1767

SPRAY EJECTED FROM THE LUNAR SURFACE

BY METEOROID IMPACT

By Donald E. Gault, Eugene M. Shoemaker,
and Henry J. Moore

Ames Research Center
Moffett Field, Calif.

NATIONAL AERONAUTICS AND SPACE ADMINISTRATION

WASHINGTON

April 1963

NATIONAL AERONAUTICS AND SPACE ADMINISTRATION

TECHNICAL NOTE D-1767

SPRAY EJECTED FROM THE LUNAR SURFACE BY METEOROID IMPACT

By Donald E. Gault, Eugene M. Shoemaker,[1] and Henry J. Moore[1]

SUMMARY

Experimentally determined mass-size distributions of fragments ejected from craters formed in rock by hypervelocity impact have been combined with estimates of the rate of impact and mass distribution of interplanetary debris which strikes the lunar surface to find the rate and mass of fragments sprayed up from the lunar surface. It is shown that the flux of particles of a given mass ejected from the lunar surface will be at least three and probably four orders of magnitude greater than the flux of the impacting interplanetary debris of the same mass. Experimentally determined distributions of mass with velocity indicate that almost all of the debris is ejected at less than lunar escape velocity (2.4 km/sec) and contributes to secondary impact events. A small fraction of the ejecta, however, will leave the lunar surface at velocities greater than the escape speed.

These results imply the presence of a lunar dust cloud of flying particles. The major fraction of the cloud is estimated to be a few kilometers deep with a spatial density at the lunar surface of the order of 10^5 to 10^7 times the spatial density of the interplanetary debris. These particles, together with the interplanetary debris, provide a powerful eroding agent that will continually abrade the lunar surface and reduce rubble to finer sizes. The inference to be drawn is that there must be at least a thin layer of dust-sized particles on the lunar surface -- a layer which is being constantly agitated and stirred by the impacts to form a heterogeneous mixture of material from the entire surface of the moon. It is to be expected that lunar probes and vehicles will be subjected to higher rates of impact when immersed in the dust cloud than during the earth-moon voyage.

INTRODUCTION

The moon, devoid of any appreciable atmosphere (ref. 1), is naked before a continuous bombardment by interplanetary debris of all sizes. The craters on the lunar surface visible to the limits of telescopic resolution are mute

[1]U.S. Geological Survey, Menlo Park, California

testimony of this bombardment by large bodies over geologic time. Öpik (ref. 2) and, most recently, Shoemaker and Hackman (ref. 3) have demonstrated that the number of what are believed to be post-mare impact craters increases exponentially with decreasing size, and Shoemaker and Hackman have shown that the size-frequency distribution is in fair agreement with the distribution for terrestrial craters of apparent meteoric origin. It is significant that the correlation between lunar and terrestrial craters depends on the mass-frequency distribution of asteroidal bodies and recovered meteorite falls (refs. 4, 5), for on this basis, by extrapolation to smaller bodies and considering the higher flux rates observed for meteors and micrometeoroids (e.g., refs. 6, 7 and 8), it is to be expected that the craters and pits formed by smaller bodies and microparticles are the primary cause of the "microscale" relief and texture of the lunar surface (refs. 9, 10). Indeed, the high flux rates for the smallest particles unimpeded by an atmosphere, probably constitute one of the principal, if not the primary, agents of erosion on the lunar surface. Meteoroid impact is, therefore, one of the major factors to be considered in the evolution of the moon to its present state, and a thorough understanding of the phenomena related to impact is essential to the study of the lunar surface.

As part of a general study of the mechanics of hypervelocity impact, Ames Research Center has undertaken an investigation of meteoroid impact in a cooperative program of research with the U. S. Geological Survey. Particular emphasis is being placed on applications to lunar problems, specifically as applied to the NASA's programs for manned and unmanned exploration of the moon. Projectiles, accelerated to velocities up to 7 km/sec in a nitrogen atmosphere of 50 to 75 mm of Hg, have been fired into various types of rock and sand targets using the light-gas gun facilities of the Ames Hypervelocity Ballistic Range. Some early results of this investigation have been reported by Shoemaker, et al. (ref. 11), and Moore, et al. (refs. 12, 13, and 14).

An important phase of the experimental program has been obtaining high-speed camera records of the ejection of material from an impact crater. Even a cursory examination of the photographic records impresses the viewer with the amount of debris ejected from a crater formed in rock. From the instant the projectile contacts the target block, a cloud of rock flour and progressively larger fragments are spewed out of the embryonic crater until the crater reaches its final dimensions. The photographic records vividly demonstrate that for each lunar impact event a tremendous number of fragments should be ejected into ballistic trajectories across the lunar surface. With a sufficiently high flux rate of interplanetary debris, one can envision a mass of fragments above the lunar surface which, continuously replenished by ejecta from subsequent impact events, would approach a steady-state cloud of impact debris. The spatial density of the ejected particles should be expected to be considerably greater than that for the interplanetary debris, particularly near the lunar surface, and the secondary impacts by the fragments should be many times more numerous than those by the interplanetary bodies.

It is the purpose of this report to present an analysis of the spray fragments ejected from the lunar surface by meteoroid impact based on data available from the joint NASA-USGS impact studies. Ejecta fragments collected from impact in rocks have been analyzed to ascertain the mass-size distribution of the

fragments. This analysis has been combined with estimates of the mass distributions of the solid material which impacts the lunar surface to give an order-of-magnitude estimate of the flux of the ejected fragments. Further, a study of ejected mass using the high-speed camera records has produced estimates for the mass-velocity distribution and velocity-ejection angle distribution of the fragments and, hence, of the spatial density and mass distribution of the ejecta across the lunar surface.

The symbols used in the text are defined in appendix A.

FLUX OF THE EJECTED FRAGMENTS

Analytical Relationships

It will be convenient first to express in analytical form the flux of fragments ejected from impact craters formed by a steady bombardment of projectiles. Empirical relationships will then be introduced to evaluate the flux of fragments from the lunar surface. Toward this end the functional forms

$$m = M_e g_1(m_e) \tag{1}$$

$$M_e = g_2(m_p) \tag{2}$$

$$f_p = g_3(m_p) \tag{3}$$

are introduced where m_e is the mass of an ejected fragment, m is the cumulative mass of the fragments with individual masses equal to or less than m_e, M_e is the total mass ejected from a crater, m_p is the mass of a projectile, and f_p is the cumulative number of projectiles (flux per unit area and time) with masses equal to or greater than m_p. Equation (1) implies that the fragmented products of an impact may be described by a simple comminution law independent of the crater dimensions. The use of this approximation for the present analysis will be discussed more fully when the empirical form of equation (1) is introduced. The second equation is based on empirical data obtained from impact-, chemical-, and nuclear-explosion cratering experiments which suggest M_e can be related to expended energy. If it is assumed that there is a characteristic impact velocity (constant specific kinetic energy) then M_e is dependent only on the projectile mass. The last, equation (3), is the form employed in the past by most investigators to describe the meteor or meteoroid population in terms of particle mass, m_p (e.g., refs. 6, 7, 8, and 15).

Now if N is defined as the cumulative number of fragments with masses equal to or greater than m_e from any one crater, then the number of fragments of mass m_e from any one crater becomes $-dN/dm_e$. The number of fragments of mass m_e from any crater can also be derived from equation (1) to be $(1/m_e)(dm/dm_e)$. By equating the two expressions, integrating, and making use of equation (2)

$$N = g_2(m_p) \int_{m_e}^{m_b} \frac{g_1'(m_e)}{m_e}\, dm_e \tag{4}$$

= the cumulative number of fragments of ejecta with masses equal to or greater than m_e formed as the result of <u>one</u> impact by a projectile of mass m_p.

The quantity m_b represents the mass of the largest fragment ejected from the crater, and the prime denotes differentiation with respect to the independent variable m_e.

The number of impacts P per unit area and time contributed by projectiles of a given mass m_p is obtained by differentiating the cumulative number of the impacting projectiles, equation (3). Thus

$$P = -\frac{df_p}{dm_p} = -g_3'(m_p)$$

and one may write

$$PN = -g_3'(m_p)g_2(m_p) \int_{m_e}^{m_b} \frac{g_1'(m_e)}{m_e}\, dm_e \tag{5}$$

= the cumulative number of ejecta fragments per unit area and time with masses equal to or greater than m_e from <u>all</u> craters resulting from the impact of projectiles of mass m_p.

Finally, when f_e is defined as the cumulative number of all ejecta fragments per unit area and time with masses equal to or greater than m_p,

$$\frac{df_e}{dm_p} = PN$$

and

$$f_e = -\int_{m_{p_1}}^{\infty} g_3'(m_p)g_2(m_p) \int_{m_e}^{m_b} \frac{g_1'(m_e)}{m_e}\, dm_e dm_p \tag{6}$$

Equation (6) is a solution for the flux of fragments with masses equal to or greater than m_e which are ejected from craters formed by a steady flux of projectiles with masses equal to or greater than m_{p_1}. It is to be noted that m_b will depend on the size of the crater; that is,

$$m_b = g_4(M_e) \tag{7}$$

and by equation (2) the upper limit for the first integration can be expressed in the terms of m_p. In addition, the lower limit for the second integral requires special consideration. No values of m_p, which produce maximum fragments m_b smaller than m_e, may be included in the integration. Therefore, when equations (2) and (7) are combined to express m_b as a function of m_p, m_b must be set equal to m_e and the resulting expression for m_{p_1} used as the lower limit of integration in the outer integral of equation (6).

Empirical Relationships

Material ejected from craters formed in rocks by the impact of hypervelocity projectiles has been collected and sieved through standard screens (e.g., ref. 16) to determine the mass-size[2] distribution of the fragments. Figure 1 is a photograph of the ejecta from a typical crater formed in basalt with the fragments separated into logarithmic sized intervals ranging from large spall plates to finely ground rock flour. Experimental mass-size distributions of ejecta from eight craters are presented in logarithmic form in figure 2 as histograms of the fractional contribution from each size class and in terms (circle symbols) of the cumulative mass of fragments smaller than a given fragment size e. For both presentations departures from linearity appear to be caused by erratic spalling of the larger fragments and by preferential fracturing along grain boundaries for the smaller fragments (ref. 12). Analysis of the debris finer than approximately 50 microns has not been completed, but results obtained to date suggest that there is a cutoff in particle size near 0.1 micron and a consequent departure from the logarithmic linearity in the sizes less than 30 microns (fig. 3). The apparent cutoff at 0.1 micron, however, may be attributable partly to incomplete collection of fine material.

Results similar to those given in figures 2 and 3 have been reported by Roberts and Blaylock (ref. 17) for the ejecta recovered from the Stagecoach series of high explosive cratering experiments in desert alluvium. Moreover, some unpublished results obtained by Shoemaker indicate that, for explosive debris in a pumiceous tuff, a linear logarithmic presentation is valid well into the micron region. To a good approximation, adequate for this analysis, the mass-size distribution of cratering events over a considerable range of expended energies may be expressed (normalized with respect to the size b of the maximum fragment)

$$m = M_e \left(\frac{e}{b}\right)^{\alpha} \tag{8}$$

[2]The size of a fragment is taken to be the intermediate dimension of the particle.

with m and M_e, as before, the cumulative and total masses ejected, e the fragment size, and α a constant. Equation (8) is the usual form employed to describe approximately the comminution of brittle, macroscopically homogeneous solids in commercial or laboratory crushing mills (e.g., ref. 18). When similar geometry for all fragments is assumed, equation (8) can be rewritten

$$m = M_e \left(\frac{m_e}{m_b}\right)^{\alpha/3} = M_e g_1(m_e) \tag{9}$$

with e and b being replaced by their respective masses, m_e and m_b as required for solution of equation (6).

A relationship between total ejected mass M_e and expended energy is shown in figure 4 which presents results from both laboratory impacts and shallow subsurface explosive cratering experiments in various media (unpublished data by Moore and refs. 19-30). The excavated mass for explosives is relatively insensitive to the physical properties of the medium but the charge burial depth is an important factor. There is no direct analogy between buried explosive and impact cratering events, but the effective scaled depth of burial λ for explosives to agree with impact data appears to be quite small ($\lambda = 0$ to 0.25) based on the total mass ejected.

Theoretical considerations (e.g., ref. 31) and experimental evidence (e.g., refs. 32 and 33) suggest that for impacts the excavated mass M_e should be directly proportional to the expended energy as shown by figure 4. However, because of the high specific energies that occur during impact at meteoric velocities, comparable to and perhaps exceeding those for the nuclear experiments, considerably more energy will be irreversibly trapped as heat and lost to the cratering processes than occurred in the events presented in figure 4. Moreover, a major fraction of the available energy from an impact is lost as kinetic energy in the ejecta squirted out at velocities up to three times the projectile velocity. For these reasons, some deviation from a direct proportionality between energy and ejected mass might be expected for impacts at meteoric velocities so the form adopted for equation (2) is

$$M_e = k_1 m_p \left(\frac{1}{2} V_i^2\right)^{\beta} = g_2(m_p) \tag{10}$$

with k_1 and β being constants and V_i the impact velocity.

The expression for $g_3(m_p)$, as indicated previously, will be taken in the form commonly used to describe the flux of meteors and meteoroids (refs. 6, 7, 8, and 15).

$$f_p = k_2 m_p^{\gamma} = g_3(m_p) \tag{11}$$

The final functional relationship $g_4(M_e)$ can be expressed

$$m_b = k_3 M_e^{\delta} = g_4(M_e) \tag{12}$$

based on the results of a correlation presented as figure 5 (unpublished data by one of the authors (Moore) and refs. 27-30, 34, and 35). In equations (11) and (12) k_2, k_3, γ, and δ are constants.

Numerical Results

Inserting equations (9) through (12) in equation (6) and carrying out the indicated integrations, one obtains for the flux of impact-spray fragments of mass equal to or greater than m_e (see appendix B)

$$f_e = k_2 K m_e^{\epsilon+\gamma} \tag{13}$$

with

$$K = k_1^{-\gamma} k_3^{-\frac{\gamma+1}{\delta}} \left(\frac{1}{2} V_i^2\right)^{-\beta\gamma} \left(\frac{\alpha\gamma}{3-\alpha}\right) \left[\frac{1}{\gamma + 1 - (\alpha\delta/3)} - \frac{1}{\gamma + 1 - \delta}\right]$$

$$\epsilon = \frac{\gamma+1}{\delta} - 1 - \gamma$$

for

$$\gamma + 1 - \frac{\alpha\delta}{3} < 0, \quad \gamma + 1 - \delta < 0, \quad \text{and} \quad \alpha \neq 3$$

Since $f_p = k_2 m_p^{\gamma}$, equation (13) can be recast in terms of the frequency of the impacting projectiles

$$f_e = K \frac{m_e^{\epsilon+\gamma}}{m_p^{\gamma}} f_p$$

and when projectiles and ejecta fragments of the same mass, m_{pe}, are considered,

$$f_e/f_p = K(m_{pe})^{\epsilon}$$

$$= \frac{\text{cumulative number of fragments with masses} \geq m_{pe}}{\text{cumulative number of projectiles with masses} \geq m_{pe}} \tag{14}$$

for unit area and time and for

$$m_e = m_p = m_{pe}$$

Seven constants (α, β, γ, δ, k_1, k_3, and V_i) and the independent variable m_{pe} are required to evaluate equation (14). Values for α range from 0.3 to 0.7 for the laboratory craters in basalt (figs. 2 and 3) and for the explosive craters in alluvium (ref. 17). The ratio f_e/f_p is relatively insensitive to α in this range and a value of α of 0.4 will be adopted. The quantity β, for reasons already cited, should be less than 1.0 and for large events may be lower than 0.88 which is suggested by empirical scaling laws for explosion craters in alluvium (ref. 36). For the present calculations, however, a value of 1.0 will be used in conjunction with a conservative value for k_1 (see fig. 4)

$$k_1 = \frac{1}{8\times10^8} \text{ gm/erg}$$

The literature on meteor and meteoroid frequencies indicates that γ, k_2, and V_i will depend on the type of projectiles being considered. The geocentric flux suggested by Hawkins (ref. 37) and Brown (ref. 4) for debris of suspected asteroidal origin is shown in figure 6 together with those of Whipple (ref. 6), Hawkins and Upton (ref. 7), and McCracken and Alexander (ref. 8) for the smaller particles usually associated with cometary and interplanetary dust. Recent results reported by Soberman and Hemenway (ref. 15) which pertain to microparticle collection with the Venus flytrap are also included for comparison assuming spherical particles with a density of 3 gm/cm^3. The values of γ and k_2 for the f_p distributions shown in figure 6 are tabulated below

Type of debris	Author	γ	$\log_{10}k_2$
Meteorites	Brown	-0.8	-16.1
Asteroids and fireballs	Hawkins	-1.0	-14.5
Meteors	Hawkins and Upton	-1.34	-12.2
Meteors	Whipple	-1.0	-11.3
Interplanetary dust	McCracken and Alexander	-1.7	-17.0
Micrometeoroids	Soberman and Hemenway	-0.4	-1.6

These values represent geocentric or near earth populations and the question arises concerning the applicability to the lunar environment. Whipple (ref. 38) has concluded that there is a geocentric concentration of the smaller particles and that the number of particles decreases as the 1.4 power of the distance from earth. At the distance of the moon from earth, Whipple finds the population of particles with masses larger than 10^{-9} grams would be about the same as that estimated for the zodiacal dust cloud, approximately three orders of magnitude less than the near earth values. Whipple's interpretation, however, has been questione by McCracken and Alexander (ref. 8) on the basis that there is no reason to suspect a priori that the mass-magnitude (visual or photographic) relationship is constant (γ = -1.0) over a large range of particle masses. The measurements of particle frequencies reported by McCracken and Alexander from satellites, probes, and sounding rockets yield γ = -1.7 directly. Hawkins and Upton's analysis also suggests that γ departs from -1.0 in support of the argument of McCracken and Alexander.

For the present analysis, fortunately, the absolute populations are not required (i.e., the value of k_2) to evaluate the ratio f_e/f_p, but only the mass distributions (i.e., γ) are required. The view adopted herein is that, regardless of any geocentric concentration, the mass distribution in the lunar environment should be essentially unchanged from near earth distributions, at least to particles of 10^{-10} grams. For smaller masses, the terrestrial atmosphere may contribute to a difference between the terrestrial and lunar distributions. The results presented by Soberman and Hemenway would seem to fall in this category and, hence, will not be employed herein. However, since the ratio f_e/f_p is quite sensitive to γ and V_i, the ratio will be evaluated for the remaining values for γ in combination with the appropriate modal velocities V_i for asteroidal and cometary debris.

Although population distributions are assumed unchanged, consideration must be given to the difference in gravitational attraction between the earth and moon as it affects the impact velocity V_i. Geocentric velocities for asteroidal debris may be taken to be 19 km/sec. While the velocities for cometary debris may be as high as 72 km/sec, a value of 30 km/sec will be employed herein as representative for most cometary material.

From the conservation of energy

$$V_i = \sqrt{2gr + V_\infty^2}$$

where g is the gravitational acceleration at the surface of a body with a radius r, and V_∞ is the approach velocity at an infinite distance from the body. The geocentric velocities, therefore, correspond to approach velocities of approximately 15 km/sec for the asteroidal debris and 28 km/sec for representative cometary material. The gravitational field of the moon contributes so small a velocity increment that impact velocities of 15 and 28 km/sec are adequate for use in equation (14).

One final set of constants δ and k_3 is required. The correlation presented as figure 5 indicates that δ has a value varying from about 1.0 for the smallest craters to 0.8 for the largest craters. A value of 1.0 will be employed for the numerical evaluations of equation (14) together with $k_3 = 10^{-1}$ for the cometary debris. Values of $\delta = 0.8$ and $k_3 = 2\times10^{-1}$ will be used for the asteroidal components. It is to be noted that a change in the relation of m_p to M_e should be expected for the larger craters ($M_e > 10^4$ grams; $m_p > 10$ grams) because of the probability of secondary breakup along pre-existing fractures or joints in the country rock, and the change of the importance of material strength with the size of ejected fragments.

A summary of the numerical reduction of equation (14) is listed in the following table:

Debris	Source	γ	V_i, km/sec	K	ϵ
Asteroids and fireballs	Hawkins	-1.0	15	1.8×10^3	0
Meteors	Whipple	-1.0	28	4.9×10^3	0
Meteors	Hawkins and Upton	-1.34	28	1.1×10^4	0
Interplanetary dust	McCracken and Alexander	-1.7	28	6.0×10^4	0

and the results are presented in graphical form as figure 7. No values are shown for Brown's distribution ($\gamma = -0.8$) because the inequality (appendix B) $\gamma + 1 - (\alpha\delta/3) < 0$ is violated with the constants required to fit this case.

The flux of the ejecta fragments is, as expected, greater in all cases than the flux of the impacting interplanetary debris. Because of the choice of constants, the exponent ϵ has a value of zero and the ratio f_e/f_p for each distribution is independent of the mass m_{pe}.

Hawkins' distribution for asteroidal projectiles gives a ratio of f_e/f_p somewhat greater than 10^3. Although the extrapolation of the small-scale laboratory experiments to the scale of the telescopically visible lunar craters is tenuous, the numerical results clearly suggest that the lunar surface is littered with large fragments thrown out of the impact craters. The great bulk of the larger fragments will, as will become evident, lie on the flanks of the craters but some can be expected at considerable distances from the points of impact. Secondary breakup, as mentioned previously, should be an important factor for large craters and it is to be expected that the ratio f_e/f_p should tend toward zero for the largest lunar craters (increasing m_{pe}).

For the smaller projectiles associated with cometary debris, the distribution of McCracken and Alexander gives an ejecta flux f_e of almost five orders of magnitude greater than the cumulative projectile flux f_p. The ratio f_e/f_p for the Hawkins and Upton distribution is approximately 10^4 while, as a lower limit for the microparticles, Whipple's distribution gives f_e larger than f_p by between three to four orders of magnitude. Thus, in all cases the secondary fragments exceed the projectile population by between 10^3 and 10^4. Since most of these fragments would be dustlike particles, a lunar dust cloud might be produced by a sufficiently high flux rate of projectiles.

DISTRIBUTION OF EJECTA FRAGMENTS ACROSS THE LUNAR SURFACE

Trajectories of Ejecta Fragments

In the absence of all but lunar gravitational forces, a fragment that is ejected from the moon and returns to the lunar surface will travel along a segment of an elliptic orbit. Except for certain limiting cases the perilune of the orbit will be within the body of the moon, and apolune will correspond to the position for maximum altitude of the fragment above the lunar surface. The circumferential distance or range R from ejection to the secondary impact is (see, e.g., ref. 39)

$$R = 2r \tan^{-1}\left(\frac{\overline{V}_e^2 \sin\theta\cos\theta}{1 - \overline{V}_e^2\cos^2\theta}\right) \tag{15}$$

where

$$0 \leq \theta \leq \pi/2$$

and

$$\bar{V}_e^2 = \frac{V_e^2}{rg_o}$$

V_e is the ejection velocity, g_o the gravitational acceleration at the lunar surface, r the lunar radius, and θ the angle of ejection measured with respect to the local horizontal. The maximum altitude h_{max} may be expressed

$$h_{max} = r \left\{ \frac{\bar{V}_e^2 - 1 + \left[1 - \bar{V}_e^2(2 - \bar{V}_e^2)\cos^2\theta\right]^{1/2}}{2 - \bar{V}_e^2} \right\} \tag{16}$$

Since r and g_o are known (1.74×10^3 km and 1.62×10^{-3} km/sec^2), the determination of the range and maximum altitude of a fragment depends only on knowledge of the vector velocity of the ejection from a crater. It is to be noted that, independent of θ, fragments are lost to the gravitational field when

$$V_e = \sqrt{2rg_o} = 2.38 \text{ km/sec}$$

As mentioned in the Introduction, high-speed camera records have been obtained of the rock fragments spewed out of impact craters and have provided a basis for estimating the mass-velocity distribution of the ejecta. The photographic records have been obtained at three nominal framing rates (10^4, 10^5, and 10^6 frames/sec) and a sequence at the highest rate is shown as figure 8. Although the total time increment covered by the record is approximately 70 microseconds, the final crater geometry in the basalt target probably has been established and only the dispersion of the larger fragments moving at relatively low speeds remains to complete the ejection sequence.

Results from an analysis of the photographic records are presented in figures 9 and 10 for aluminum spheres (1/16- and 1/8-inch diameter) impacting at normal incidence on basalt at a nominal velocity of $V_i = 6.25$ km/sec. Figure 9 presents the ejection velocity V_e as a function of the ejection angle θ, and figure 10 presents the cumulative mass $\bar{m}$ which is ejected with velocities in excess of V_e. Material ejected at the highest velocities ($V_e \approx 19$ km/sec) and lowest angles ($\theta < 20^\circ$) is believed to be associated with a jet emanating from the interface between the projectile and target (see, e.g., refs. 40, 41, and 42). Subsequent to the jetting the ejection velocity quickly decays to very small values and the main mass of fragments leaves the craters with velocities less than 0.5 km/sec and with θ greater than 45°. The discontinuous variation in the cumulative mass with velocity is believed to be associated with a transition from plastic to elastic flow behind the shock front which propagates outward from the point of impact.

Estimates for the distribution of mass with velocity for the 15 and 28 km/sec impact velocities are also included in figures 9 and 10. In extrapolating the laboratory results to higher impact velocities, it is convenient to assume that the expended energy remained constant ($1/2 m_p V_i^2 \approx 9 \times 10^9$ erg). Thus the total ejected mass M_e becomes independent of the impact velocity (eq. (10)) and the projectile mass m_p can be considered to vary inversely with the square of the impact velocity V_i. Moreover, since the main bulk of the debris is ejected under conditions of elastic flow, the absolute values for the ejection velocity V_e were considered essentially independent of the impact velocity except for a small fraction of the ejected mass associated with jetting and plastic flow. It is to be expected that, since jetting is a hydrodynamic process, the velocity and mass of the jetted material will scale approximately linearly with some characteristic velocity and the cube of a characteristic length (i.e., projectile mass), respectively. Thus, the maximum ejection velocities for 15 and 28 km/sec in figures 9 and 10 have been scaled by taking $V_{e_{max}} = (V_i/6.25)$ while the associated jetted masses in figure 10 have been scaled by $\bar{m}_{min} = (6.25/V_i)^2$. The calculated end points for jetting and the experimentally determined curves have been joined arbitrarily to complete the velocity-ejection angle relationships and the cumulative mass-velocity distributions for the higher impact velocities.

It should be cautioned that the above procedure neglects any effects of the increase in specific kinetic energy for the higher impact velocities. An increase in impact velocity increases the fraction of the kinetic energy which is trapped irreversibly as heat during the shock compression of the projectile and target media. Thus, even though the kinetic energy may remain constant, the fraction of energy available for crushing and ejection of fragmented material decreases with an increase in impact velocity and one should expect a slight decrease in the total ejected mass M_e. The effect would be to translate the estimated mass-velocity distributions shown in figure 10 to the left and reduce the cumulative masses which are ejected at velocities in excess of any given ejection velocity. The over-all change is believed to be small, but it should be kept in mind that results presented herein for 15 and 28 km/sec may represent the maximum mass which can be ejected at any given velocity.

Distribution of Ejecta Fragments in the Lunar Environment

The circumferential distance ejected fragments will travel across the moon from an impact crater (derived from the estimated variation of cumulative mass with vector velocity and from eq. (15)), is presented in figure 11 as the normalized cumulative mass $\bar{m}/m_p$ that contributes to secondary impact events beyond a given distance from the point of projectile impact. Similarly, with the use of the experimental data and equation (16), the apolune distance of the ejected fragments is presented in figure 12 as the normalized cumulative mass $\bar{m}/m_p$ of the ejected fragments ejected above a given lunar altitude. Three curves are shown in the presentations, one derived directly from the experimental data for a nominal impact velocity of 6.4 km/sec and estimates for 15 km/sec and 28 km/sec impact velocities.

The results presented in figures 11 and 12 indicate that the main fraction of the ejecta, say 90 percent, will never exceed an altitude of the order of 10 kilometers and will return to the lunar surface within a radius of the order of 30 kilometers from the point of impact. If one considers virtually all of the ejecta mass (99 percent), the maximum altitude and radial distance increase to 30 and 150 kilometers, respectively.

The flux of the ejected fragments has been found to be from 10^3 to almost 10^5 times the flux of the interplanetary debris (fig. 7). Since the velocities of the bulk of the ejected fragments are some two orders of magnitude less than the velocities of the projectiles, it follows that the spatial density of the ejecta at the lunar surface is from 10^5 to 10^7 times the spatial density of the impacting interplanetary debris.

The last 1 percent of the ejected mass includes perhaps the most significant fraction of the fragments. Dependent on the impact velocity, a mass of fragments equivalent to several projectile masses is ejected at velocities in excess of lunar escape velocity and is lost to the lunar gravitational field. It is interesting to note in this connection that the impact experiments and analysis herein for impact into solid basalt indicate that the velocity for which the mass lost from the moon is equal to the acquired projectile mass is between 9 and 10 km/sec. Thus, it appears that all asteroidal and cometary projectiles are effective in removing mass from the moon.

DISCUSSION

The results from the present study indicate the existence of a lunar "atmosphere" of high-speed ejecta. Moreover, the results suggest that the lunar surface material is composed of a mixed rubble of unsorted rock fragments ranging in size from large blocks to submicron sized particles. A model of the lunar surface in which a gravelly material extends to depths of at least several meters has been proposed recently by Baldwin (ref. 43) based on observations of the thermal radiation from the moon. In view of the higher flux rates for the smallest projectiles, both interplanetary solids and crater ejecta, it is to be expected that the surface rubble is continually abraded to finer sizes and that over geologic time small voids and cracks have gradually filled with pulverized rock. Indeed the abrasive action of the "atmosphere" must contribute, again consistent with optical and radio telescope observations, to at least a thin mantle of fine particles over the entire lunar surface--a layer which is constantly agitated and stirred by impact to form a heterogeneous mixture of mare and terra material.

A question immediately arises concerning the applicability of the current analysis, based on impact in solid targets, to impact in an unconsolidated or weakly cemented particulate medium. Some results for craters formed in a weakly bonded quartz sand (crushing strength approximately 10^7 dynes/cm^2) are shown in figure 4 by the filled symbols. Sand particles with a grain size of 0.3 mm were employed for these tests in combination with projectiles which had a diameter of 1/8 inch (3.18 mm). For a given expended energy, the mass M_e ejected from a

crater in the bonded sand exceeds the mass from the craters in basalt by a factor of at least three. In addition, the material sprayed out from the craters in sand contains few, if any, large spalls and consists almost entirely of finely crushed quartz, disaggregated sand grains, and a few clusters of sand grains welded together with fused material (silica). Both the increased mass M_e and the lack of spalls will serve to increase the calculated values of f_e/f_p over those based on the solid targets. The increase would be about an order of magnitude for McCracken and Alexander's distribution ($\gamma = -1.7$) and a factor of, perhaps, four for Whipple's distribution ($\gamma = -1.0$). On this basis the numerical values for f_e/f_p in figure 7 should be conservative.

There is, however, no assurance that the data presented in figure 4 for impact in sand are valid when the projectile is small relative to the grain size of the target and/or the target material is a diffuse low-density medium, such as that suggested by D. D. Cudaback (ref. 44) for the lunar surface. It is probable that for these latter conditions less mass and fewer fragments will be ejected by an impact as compared to an equivalent event in a solid rock. This would tend, of course, to reduce the effectiveness of the smaller particles of interplanetary debris in producing secondary fragments. Any reduction should be offset by the increases noted in the previous paragraph but a quantitative evaluation of the combined effects integrated over a spectrum of projectile masses cannot be made at the present time. It is worth noting, however, that the ratio of projectile to sand-grain dimensions for the data in figure 4 is the same as that which would occur with a lunar dust layer consisting of 1 micron particles and 10^{-9} gram interplanetary projectiles (10 micron diameter, 3 g/cc density).

One difference observed between impact in rock and sand is a change in the velocity-ejection angle distribution of the fragments from that shown in figure 9. Based on the results currently available for impact in sand, the ejection angle θ increases rapidly from the low values associated with jetting, attains a peak value, and then decreases monotonically to some minimum value. Such a variation in θ will increase the range R and decrease the apolune height h_{max} from that shown in figures 11 and 12 for an undetermined fraction of the low-speed ejecta. This difference in the ejection angles, attributable to reduced target strength, does not introduce any important changes to the analysis and, in particular, will not change the previous estimates of the ratio f_e/f_p or the spatial density of the ejecta fragments at the lunar surface.

A lunar atmosphere of high-speed projectiles poses a hostile environment for both manned and unmanned exploration of the moon. The frequency of impacts on manned vehicles and instrumented probes will be far greater on the moon than that encountered during the earth-moon voyage. The secondary impacts should not greatly increase the hazard from catastrophic punctures, because the bulk of the ejected material travels at low speeds, but the abrasive action of the multiple impacts, even at low speed, may present operational and maintenance problems for optical and solar-cell surfaces. Multiple impacts will steadily degrade such surfaces, and with sufficiently high rates of impact, may appreciably shorten the useful lifetime of the related equipment and experiments. Unfortunately, an estimate of the degradation cannot be made with any confidence at the present time because of the uncertainties in the absolute values for the flux of interplanetary solids onto the moon. With reference to figure 7, this can be demonstrated by

Whipple's flux distribution (ref. 6) and interpretation of satellite micrometeoroid measurements (ref. 20); one obtains an absolute flux and a spatial density for secondary particles having masses greater than 10^{-10} grams of the order of one particle per second over an area of approximately 10 square meters and one particle per 10^3 cubic meters, respectively. In contrast, the direct application of McCracken and Alexander's results (ref. 8) yields an impact rate and spatial density almost six orders of magnitude higher--10 impacts per second per square centimeter and one particle per 10^3 cubic centimeters, repectively. The lowest rate might be considered minor as compared to the highest rate. The actual values are probably somewhere between the two extremes,[3] but it remains for impact counters in the lunar environment to establish the rate at which ejecta are thrown up by the impact of interplanetary solids. It is, perhaps, superfluous to note that the investigation of impact on and near the lunar surface is a prerequisite to the undertaking of manned exploration of the moon.

CONCLUDING REMARKS

The analysis of the distribution of solid material thrown out of impact craters on the moon has ramifications which extend well beyond the scope of the present paper. Nevertheless, it should be mentioned in closing that the implications arising from the indicated negative accretion of mass by the moon are particularly significant. An effectively steady rate of ejection of an appreciable mass of solids from the lunar environment over geologic time is fundamentally important both as an evolutionary process which has brought the moon to its present state and as an origin for some of the solid debris in interplanetary space. The latter, of course, has a direct bearing on many problems, notably the zodiacal dust, the gegenschein, the Kordelewski clouds, and any geocentric concentration of dust. Moreover, the possibility of ejecting several projectile masses of material away from the gravitational field of the moon provides an origin for some meteorites. It is interesting to note, also, that impact appears to be an extremely efficient mechanism for the levitation of small particles above the lunar surface which is necessary in Gold's theory for a space-charge fluidization and transport of dust on the moon. These and other related problems serve to emphasize the role of lunar impact as one of the important keys to the exploration and better understanding of the solar system.

Ames Research Center
National Aeronautics and Space Administration
Moffett Field, Calif., Dec. 27, 1962

---

[3]John A. O'Keefe, NASA Goddard Space Flight Center, has pointed out (private communication) that the light scattered by a dust cloud corresponding to the highest impact rate should provide a readily detectable extension of the lunar cusps near first quarter. No such extension has been observed. Refined photometric techniques should be capable of detecting a lunar dust cloud some three to five orders of magnitude less dense than that corresponding to the highest flux rate estimated above.

APPENDIX A

SYMBOL NOTATION

The principal symbols employed throughout the body of the text are summarized as follows:

b	size of largest fragment ejected from a crater
d	explosive burial depth, ft
e	size of fragment ejected from a crater
E	expended energy expressed in pounds of TNT
f_e	flux of fragments per unit area and time which have masses equal to or greater than m_e
f_p	flux per unit area and time of interplanetary debris which have masses equal to or greater than m_p
g_o	gravitational acceleration at the surface of the moon
h_{max}	maximum altitude a fragment attains above the lunar surface (apolune)
K, k_1, k_2, k_3	constants introduced in equations (10) through (13)
m	cumulative mass of fragments with masses equal to or less than m_e
$\overline{m}$	cumulative mass of fragments ejected from a crater with velocities equal to or greater than V_e
m_b	mass of largest fragment from a crater
m_e	mass of fragment from a crater
m_p	mass of projectile or interplanetary debris
m_{pe}	mass of fragment and projectile when $m_e = m_p = m_{pe}$
M_e	mass of material excavated from a crater
r	radius of moon or planet
R	circumferential range of fragment ejected from a crater
V_e	ejection velocity
V_i	impact velocity

V_∞ velocity of the interplanetary debris at an infinite distance from the moon or planet

$\bar{V}_e$ $V_e/\sqrt{rg_o}$

$\alpha,\beta,\gamma,\delta,\epsilon$ constants introduced in equations (10) through (13)

θ ejection angle of fragment with respect to the local horizontal

λ scaled depth of explosion, $d/E^{1/3}$

The cgs system is employed throughout except where noted.

APPENDIX B

EVALUATION OF EQUATION (7) BY USE OF EMPIRICAL RELATIONSHIPS

The flux of fragments ejected from craters formed by a steady flux of projectiles with mass $\infty > m_p \geq m_{p_1}$ is expressed in equation (7) as

$$f_e = -\int_{m_{p_1}}^{\infty} g_3'(m_p) g_2(m_p) \int_{m_e}^{m_b} \frac{g_1'(m_e)}{m_e} \, dm_e dm_p \tag{B1}$$

and the empirical relationships which will be used in evaluating this equation (eqs. (9) through (12)) are

$$g_1(m_e) = \left(\frac{m_e}{m_b}\right)^{\alpha/3} \tag{B2}$$

$$g_2(m_p) = k_1 m_p \left(\frac{1}{2} V_i^2\right)^{\beta} = M_e \tag{B3}$$

$$g_3(m_p) = k_2 m_p^{\gamma} = f_p \tag{B4}$$

$$g_4(M_e) = m_b = k_3 M_e^{\delta} = k_3 \left[k_1 m_p \left(\frac{1}{2} V_i^2\right)^{\beta}\right]^{\delta} \tag{B5}$$

Using equations (B2) to (B4) in (B1), one obtains

$$f_e = -\frac{\alpha}{3} \gamma k_1 k_2 \left(\frac{1}{2} V_i^2\right)^{\beta} \int_{m_{p_1}}^{\infty} m_p^{\gamma} \int_{m_e}^{m_b} \frac{m_e^{(\alpha/3) - 2}}{m_b^{(\alpha/3)}} \, dm_e dm_p$$

After the first integration

$$f_e = -\frac{\alpha}{\alpha - 3} \gamma k_1 k_2 \left(\frac{1}{2} V_i^2\right)^{\beta} \int_{m_{p_1}}^{\infty} m_p^{\gamma} \left[\frac{m_b^{(\alpha/3) - 1} - m_e^{(\alpha/3) - 1}}{m_b^{(\alpha/3)}}\right] dm_p \tag{B6}$$

provided that $\alpha \neq 3$. For the data in this report and in reference 17, α is less than one. Equation (B5) can be used to recast equation (B6) into

$$f_e = C_1 \int_{m_{p_1}}^{\infty} \left(C_2 m_p^{\gamma - \delta} - m_p^{\gamma} - \frac{\alpha\delta}{3} m_e^{\frac{\alpha}{3} - 1}\right) dm_p \tag{B7}$$

with

$$C_1 = \left(\frac{\alpha\gamma}{3 - \alpha}\right) k_1^{1 - \frac{\alpha\delta}{3}} k_2 k_3^{-\frac{\alpha}{3}} \left(\frac{1}{2} V_i^2\right)^{\beta \left(1 - \frac{\alpha\delta}{3}\right)}$$

$$C_2 = \left\{ k_3 \left[k_1 \left(\frac{1}{2} V_i^2\right)^{\beta} \right]^{\delta} \right\}^{(\alpha/3)-1}$$

Since no projectiles may be included in the final integration which would produce fragments $m_b < m_e$, equation (B5) is rewritten in terms of m_e and m_{p_1}

$$m_b = m_e = k_3 \left[k_1 m_{p_1} \left(\frac{1}{2} V_i^2\right)^{\beta} \right]^{\delta}$$

so that

$$m_{p_1} = \left(\frac{m_e}{k_3}\right)^{1/\delta} \left[k_1 \left(\frac{1}{2} V_i^2\right)^{\beta} \right]^{-1} \tag{B8}$$

= mass of the projectile which produces a maximum fragment with $m_b = m_e$

Integration of equation (B7) using the equality of equation (B8) in the lower limit gives

$$f_e = k_2 K m_e^{\epsilon+\gamma} \tag{B9}$$

with

$$K = k_1^{-\gamma} k_3^{-\frac{\gamma + 1}{\delta}} \left(\frac{1}{2} V_i^2\right)^{-\beta\gamma} \left(\frac{\alpha\gamma}{3 - \alpha}\right) \left[\frac{1}{\gamma + 1 - (\alpha\delta/3)} - \frac{1}{\gamma + 1 - \delta} \right]$$

$$\epsilon = \frac{\gamma + 1}{\delta} - 1 - \gamma$$

for

$$\gamma + 1 - \frac{\alpha\delta}{3} < 0, \quad \gamma + 1 - \delta < 0$$

The two inequalities are a mathematical restriction that arises as a consequence of the form of expression employed to describe the flux of interplanetary debris (eq. (B4)) and the final integration to bodies of infinite mass (eq. (B7)). This

can be illustrated by differentiating equation (B4) to obtain the number of interplanetary projectiles P having a mass m_p

$$P = -\frac{df_p}{dm_p} = -\gamma k_2 m_p^{\gamma-1} \tag{B10}$$

The over-all mass of the bodies whose individual masses are m_p is

$$m_p P = -\gamma k_2 m_p^{\gamma}$$

and the total or integrated mass of all the bodies with masses greater than m_p becomes

$$\text{Total mass} = -\gamma k_2 \int_{m_p}^{\infty} m_p^{\gamma} dm_p \tag{B11}$$

When $\gamma < -1$, a finite mass is obtained and with $\gamma \geq -1$, an infinite mass results.

Physically, equations (B10) and (B11) indicate that for $\gamma < -1$, the number of particles and their mass increase without limit as m_p tends to zero, while for $\gamma \geq -1$, the number of bodies decreases but the masses involved increase without limit as m_p tends to infinity. Thus, the latter implies (through eq. (B3)) an infinite mass excavated for the lunar impacts and an infinite number of secondary fragments. The specified inequalities for equation (B9) are directly related to this limitation in the mathematical development. The limitation can be circumvented, of course, by specifying a finite upper limit in equation (B7), but the added complexity is not justified for the present analysis.

12. Moore, H. J., Gault, D. E., Lugn, R. V., and Shoemaker, E. M.: Hypervelocity Impact of Steel Into Coconino Sandstone. Proc. of the Geophysical Laboratory, Lawrence Radiation Laboratory, Cratering Symposium, UCRL-6438, Part II, Paper N, 1961, pp. N-1 to N-23.

13. Moore, H. J., Gault, D. E., and Lugn, R. V.: Experimental Hypervelocity Impact Craters in Rock. Proc. of the 5th Hypervelocity Impact Symposium, Denver, 1961.

14. Moore, H. J., Gault, D. E., and Lugn, R. V.: Impact Craters in Basalt. Abstract in Pacific Southwest Mineral Conference of AIME, San Francisco, 1962, p. 17.

15. Soberman, R. K., and Hemenway, C. L.: Micrometeorite Collection From a Recoverable Sounding Rocket. GRD Research Note 71, R. K. Soberman, ed., Article III, Nov. 1961, pp. 41-50.

16. Anon.; The Profitable Use of Testing Sieves. The W. S. Tyler Co., Catalogue 53, 1957 edition.

17. Roberts, Wayne A., and Blaylock, John A.: Distribution of Debris Ejected by the Stagecoach Series of High Explosive Cratering Bursts. Boeing Airplane Co., Document D2-6955-1, 1961.

18. Schuhmann, R., Jr.: Principles of Comminution, I - Size Distribution and Surface Calculations. Mining Technology, vol. 4, no. 4, July 1940, pp. 1-11.

19. Maurer, W. C., and Rinehart, J. S.: Impact Crater Formation in Rock. Proc. of 4th Hypervelocity Impact Symposium, Eglin Air Force Base, Florida, vol. 3, Paper 32, April 1960.

20. Hartman, Howard L.: Basic Studies of Percussion Drilling. Mining Engr., vol. 11, no. 1, Jan. 1959, pp. 68-75.

21. Johnson, G. W.: Mineral Resource Development by the Use of Nuclear Explosives. Rep. 5458, Lawrence Radiation Lab., Univ. of Calif., 1959, p. 10.

22. Murphey, Byron F.: High Explosive Crater Studies: Desert Alluvium. SC 4614 (RR), Sandia Corp., May 1961.

23. Sachs, D. C., and Swift, L. M.: Small Explosion Tests, Project Mole, Vols. I and II. Stanford Research Inst. Proj. PU-876. Final Rep. AFSWP-291.

24. Shelton, A. Vay, Nordyke, Milo D., and Goeckermann, Robert H.: The Neptune Event, A Nuclear Explosive Cratering Experiment. Rep. 5766, Lawrence Radiation Lab., Univ. of Calif., Apr. 19, 1960, pp. 3-5.

25. U. S. Corps of Engineers: Cratering Effects of Surface and Buried HE Charges in Loess and Clay. Tech. Rep. 2-482, Waterways Experiment Station, Corps of Engineers, Vicksburg, Miss., June 1958.

REFERENCES

1. Elsmore, B.: Radio Observations of the Lunar Atmosphere. Phil. Mag., Eighth Series, vol. 2, no. 19, Aug., 1957, pp. 1040-1046.

2. Öpik, E. J.: The Lunar Surface as an Impact Counter. Irish Astr. Jour., vol. 120, no. 5, 1960, pp. 404-411.

3. Shoemaker, Eugene M., Hackman, Robert J., and Eggleton, Richard E.: Interplanetary Correlation of Geologic Time. Preprint 61-7, 7th Annual Meeting American Astronautical Society, April 1961.

4. Brown, Harrison: The Density and Mass Distribution of Meteoritic Bodies in the Neighborhood of the Earth's Orbit. Jour. Geo. Res., vol. 65, no. 6, June 1960, pp. 1679-1683. (See also Addendum: The Density and Mass Distribution of Meteoritic Bodies in the Neighborhood of the Earth's Orbit. Jour. Geo. Res., vol. 66, no. 4, April 1961, pp. 1316-1317.)

5. Kuiper, G. P., Fujita, Y., Gehrels, T., Groeneveld, I., Kent, J., Van Biesbroeck, G., and Van Houten, C. J.: Survey of Asteroids Astrophysical Jour., Supplement Series no. 32, vol. III, July 1958, pp. 289-428.

6. Whipple, Fred L.: Meteoritic Risk to Space Vehicles. Vistas in Astronautics; First Annual Air Force Office of Scientific Research Astronautics Symposium, Pergamon Press, N. Y., 1958, pp. 115-124.

7. Hawkins, G. S., and Upton, E. K. L.: The Influx Rate of Meteors in the Earth's Atmosphere. Astrophysical Jour., vol. 128, no. 3, 1958 pp. 727-735.

8. McCracken, C. W., and Alexander, W. M.: The Distribution of Small Interplanetary Dust Particles in the Vicinity of Earth. Preprint, International Symposium on the Astronomy and Physics of Meteors, Cambridge, Mass., 28 August - 1 September, 1961.

9. Barabashov, N. P.: Structure of the Moon's Surface and Investigation of the First Photographs of Its Far Side. NASA Translation of "Struktura poverkhnosti Luny i issledovaniye pervykh fotografiy yeye obratnoy storony." NASA TT F-8117.

10. Salisbury, John W., and Campen, Charles F., Jr.: Location of a Lunar Base. GRD Research Note 70, 1961.

11. Shoemaker, E. M., Gault, D. E., and Lugn, R. V.: Shatter Cones Formed by High Speed Impact in Dolomite. U. S. Geological Survey Professional Paper 424-D, 1961, pp. 365-367.

26. Vortman, L. J., Chabai, A. J., Perret, W. R., and Reed, J. W.: Project Buckboard. SC-4486 (RR), Sandia Corp., Nov. 1960.

27. Kachadoorian, Reuben: Geologic Results of November 1960 Project Chariot High-Explosive Cratering Experiment, Cape Thompson, Alaska. U. S. Geol. Survey Prof. Paper 424-D, 1961, pp. D-368 - D-371.

28. Duvall, W. I., and Atchison, T. C.: Rock Breakage by Explosives. U. S. Bureau of Mines Rep. Inv. 5356, 1957. p. 52.

29. Gilbert, G. K.: The Origin of Hypothesis, Illustrated by the Discussion of a Topographic Problem. Science, n.s., vol. 3, no. 53, 1896, p. 13.

30. Nininger, H. H., and Huss, Glenn I.: The Unique Meteorite Crater at Dalgaranga, Western Australia. Mineralogical Mag., vol. 32, no. 251, Sept. 1960, pp. 619-639.

31. Charters, A. C., and Summers, James L.: Comments on the Phenomena of High-Speed Impact. NOLR1238, U. S. Naval Ordance Lab., White Oak, Silver Spring, Md., May 25-26, 1959, pp. 200-221.

32. Summers, James L.: Investigation of High-Speed Impact: Regions of Impact and Impact at Oblique Angles. NASA TN D-94, 1959.

33. Kineke, John H., Jr.: Observations of Crater Formation in Ductile Materials. Proc. Fifth Symposium on Hypervelocity Impact, vol. 1, pt. 2, Denver, Oct. 30 - Nov. 1, 1961, pp. 339-370.

34. Branco, W., and Fraas, E.: Das vulcanische Ries bei Nördlingen in seiner Bedeutung fur Fragen der allgemeinen Geologie. K. Preussische Akademie der Wissenschaffen, Physikalisch-mathematische Klasse, Abhandlungen, 1901, pp. 1-69.

35. Dorn, Paul: Ein Jahrhundert Ries Geologie. Deutsche Geologische Gesellschaft Zeitschrift, vol. 100, 1950, pp. 348-365.

36. Chabai, A. J., and Hankins, D. M.: Gravity Scaling Laws for Explosion Craters. SC-4541 (RR), Sandia Corp., Dec. 1960.

37. Hawkins, Gerald S.: The Relation Between Asteroids, Fireballs and Meteorites. Astronomical Jour., vol. 64, no. 1275, Dec. 1959, pp. 450-454.

38. Whipple, Fred L.: The Dust Cloud About the Earth. Nature, vol. 189, no. 4759, Jan. 14, 1961, pp. 127-128.

39. Whittaker, E. T.: A Treatise on the Analytical Dynamics of Particles and Rigid Bodies. Dover Pub., N. Y., 1944.

40. Walsh, J. M., Shreffler, R. G., and Willig, F. J.: Limiting Conditions for Jet Formation in High Velocity Collisions. Jour. Appl. Phys., vol. 24, no. 3, March 1953, pp. 349-359.

41. Birkhoff, Garrett, MacDougall, Duncan P., Pugh, Emerson M., and Taylor, Geoffrey: Explosives With Lined Cavities. Jour. Appl. Phys., vol. 19, June 1948, pp. 563-582.

42. Allen, William A., Morrison, Harvey L., Ray, Daniel B., and Rogers, James W.: Fluid Mechanics of Copper. The Physics of Fluids, vol. 2, no. 3, May-June 1959, pp. 324-333.

43. Baldwin, J. E.: Thermal Radiation From the Moon and the Heat Flow Through the Lunar Surface. Monthly Notices of the Royal Astronomical Society, vol. 122, no. 6, 1961, pp. 513-522.

44. Perlman, David: The Cotton Candy Coating on the Moon. San Francisco Chronicle, Oct. 29, 1962, p. 14.

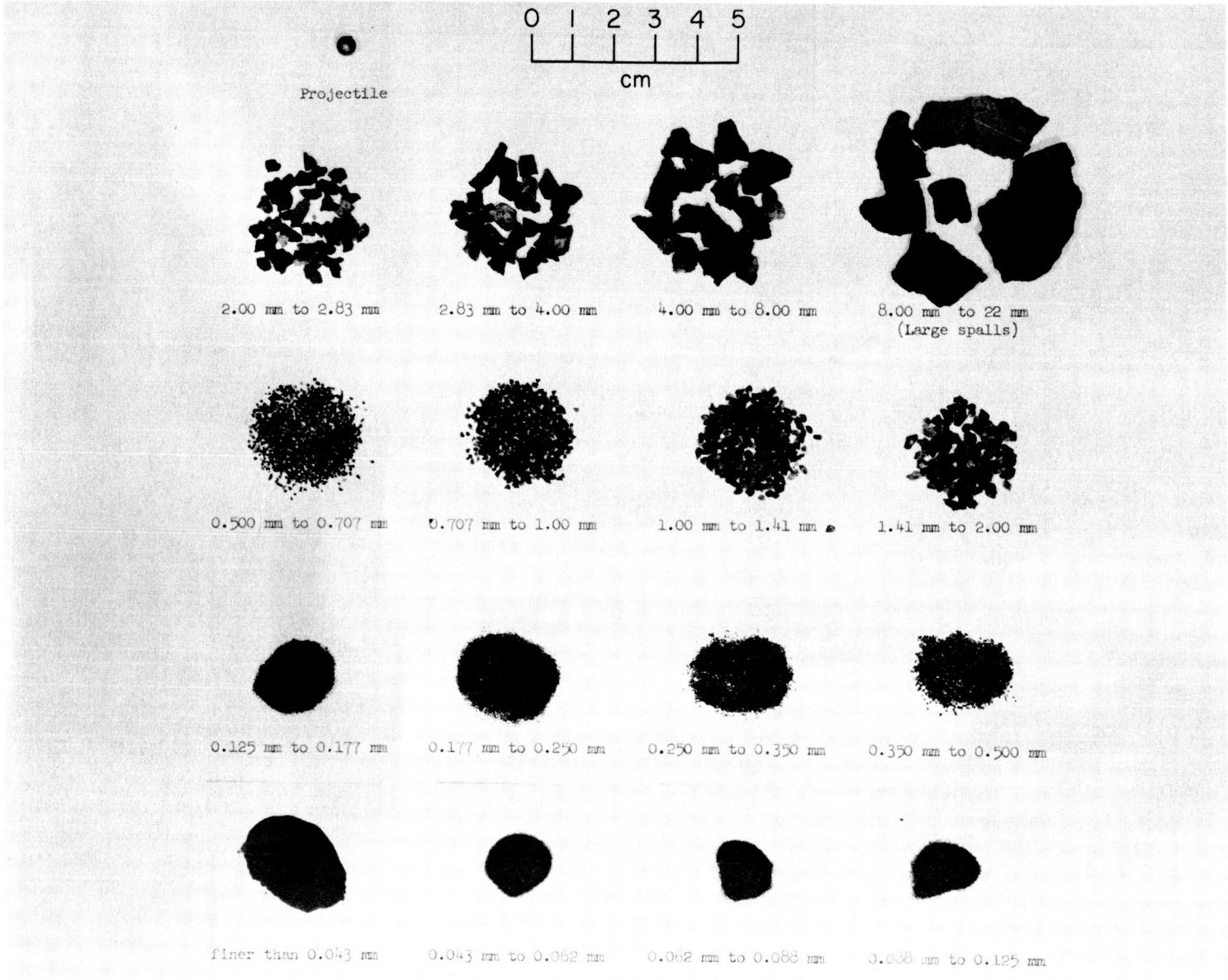

A-29661

Figure 1.- Ejecta from a typical crater formed in basalt with fragments separated into logarithmic-sized intervals.

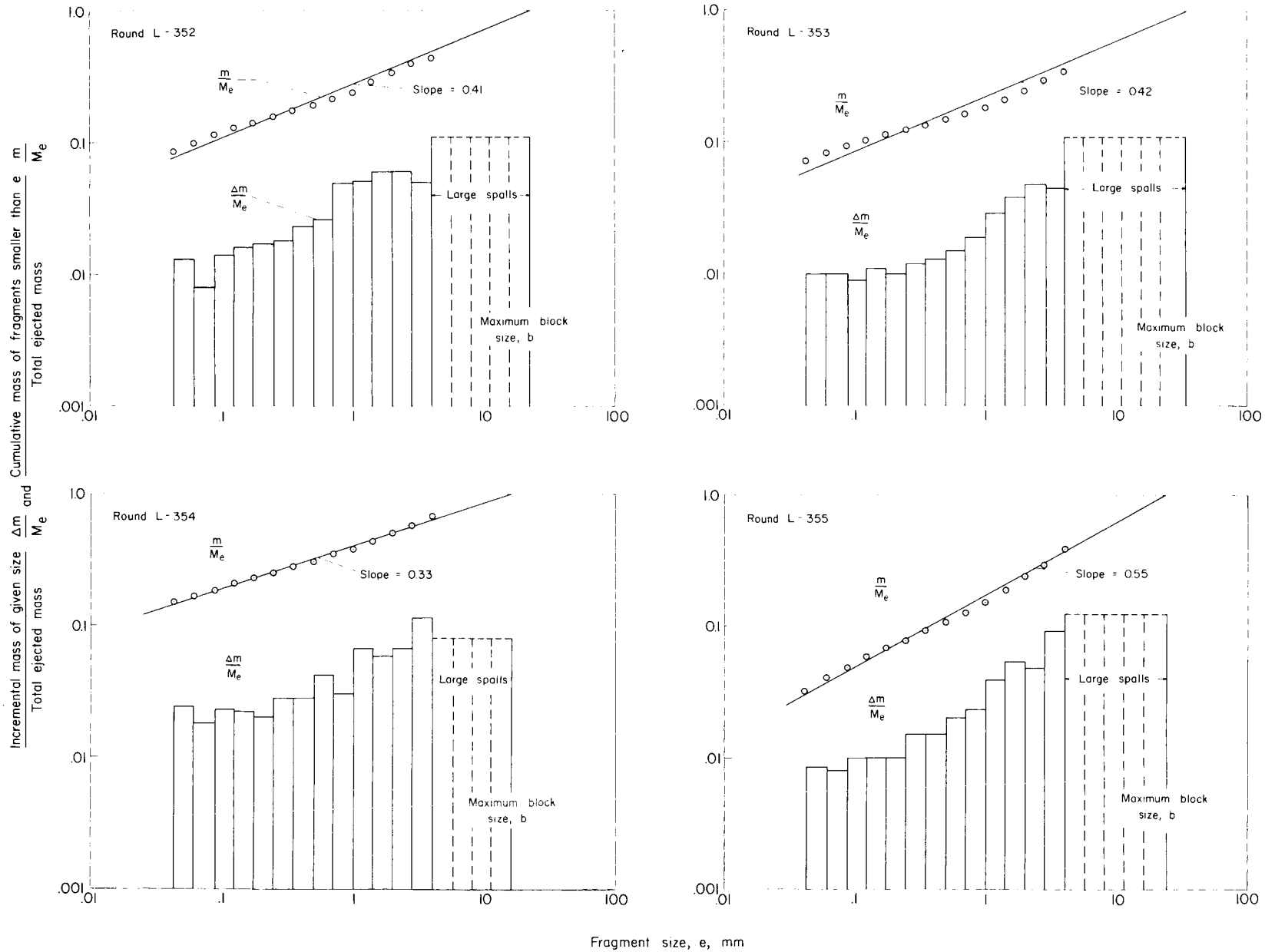

Figure 2.- Mass-size and cumulative mass-size distributions of fragmented rock from craters formed in basalt by hypervelocity impact.

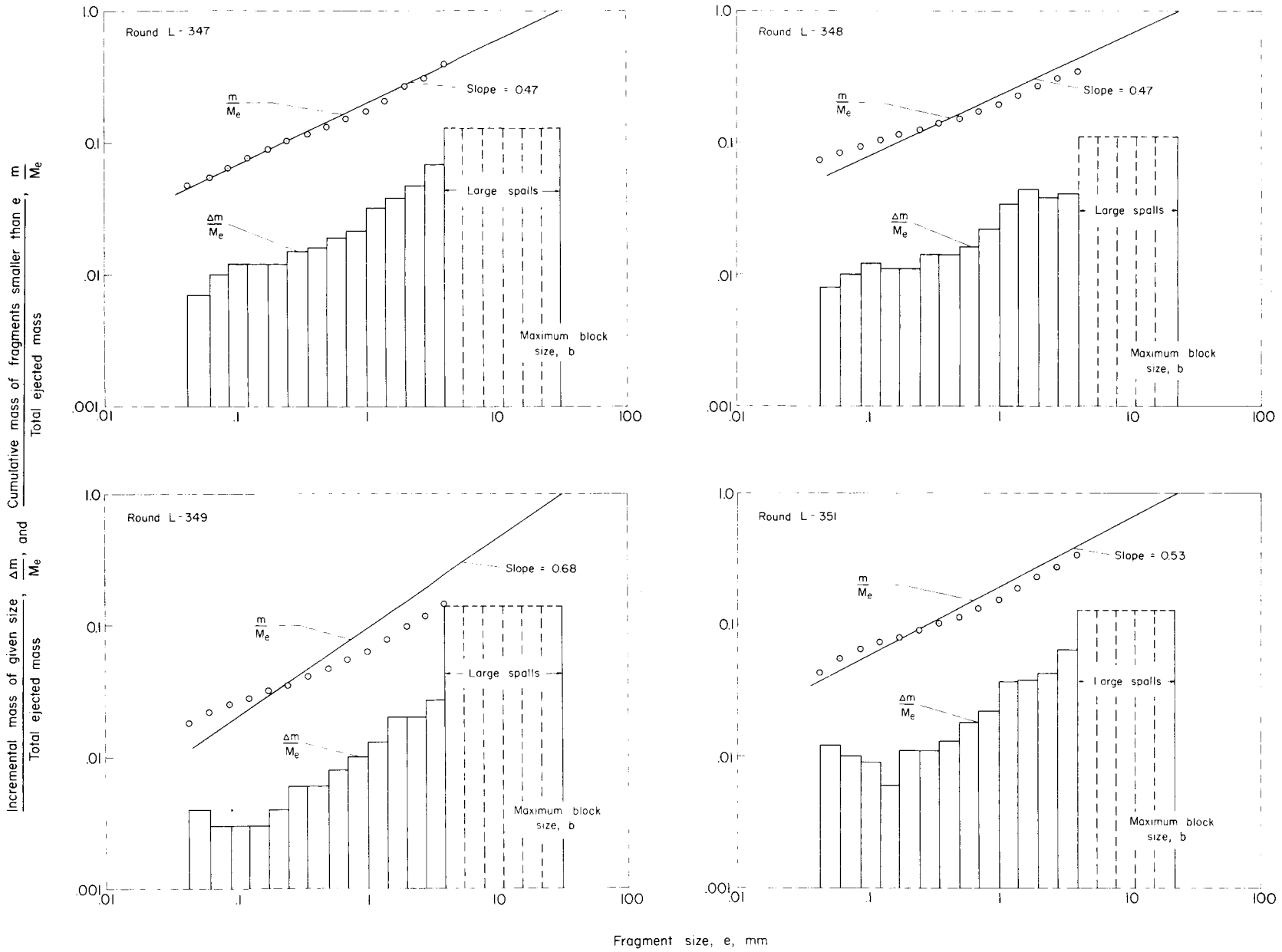

Figure 2.- Mass-size and cumulative mass-size distributions of fragmented rock from craters formed in basalt by hypervelocity impact - Concluded.

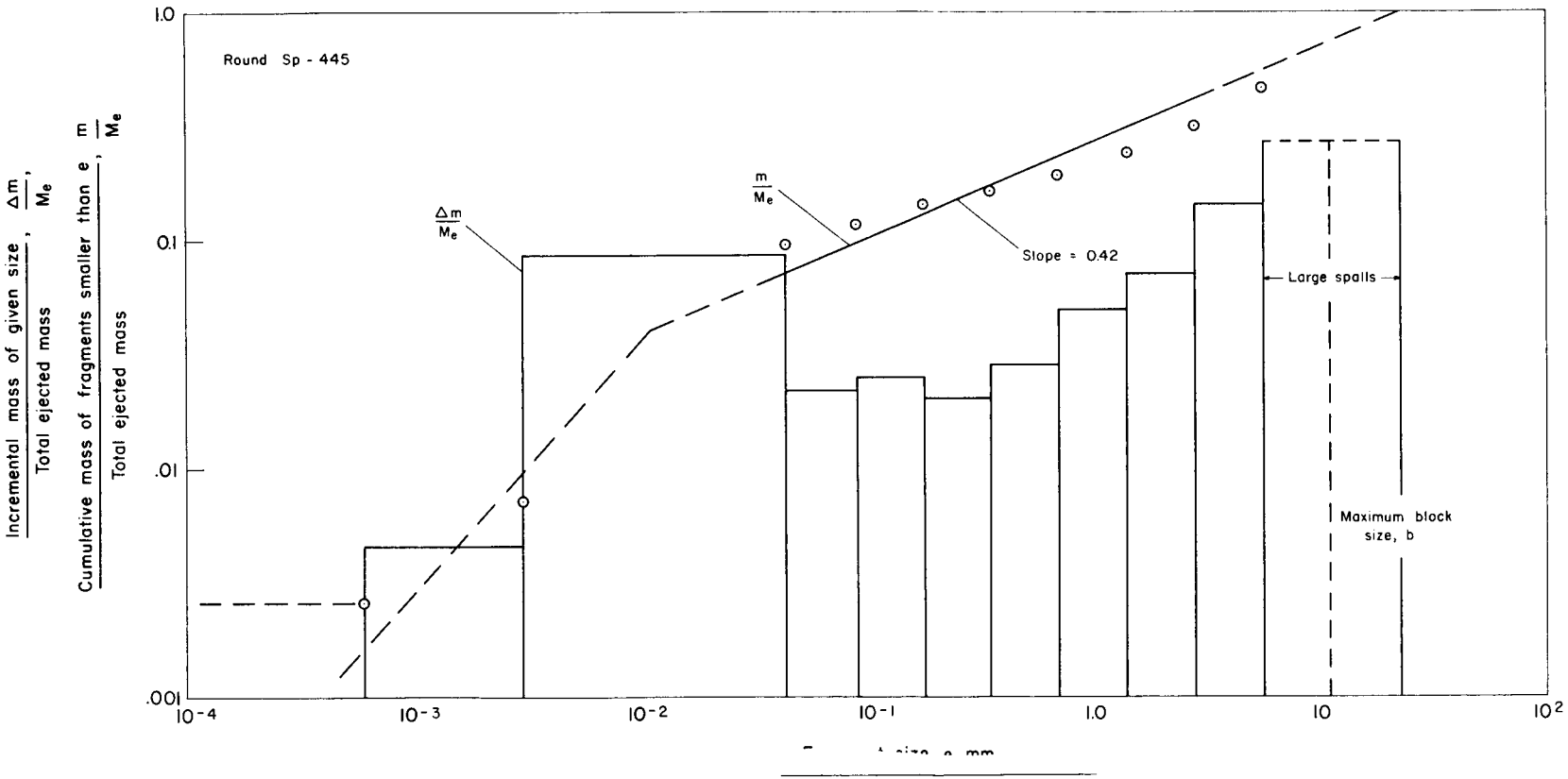

Figure 3.- Mass-size and cumulative mass-size distributions of fragmented rock from a crater formed in basalt by hypervelocity impact.

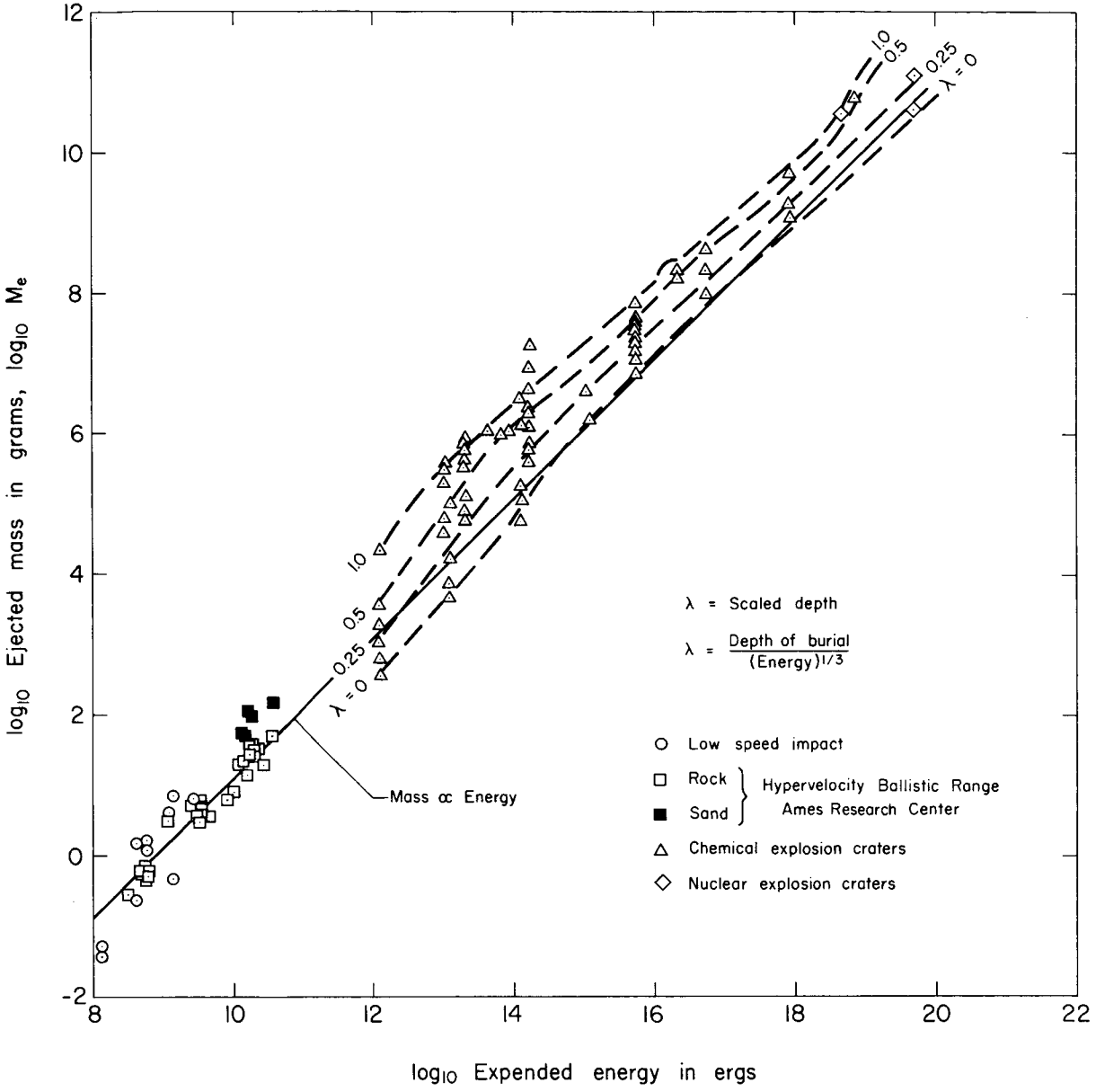

Figure 4.- Correlation of the total ejected mass with expended energy for explosive and impact cratering events.

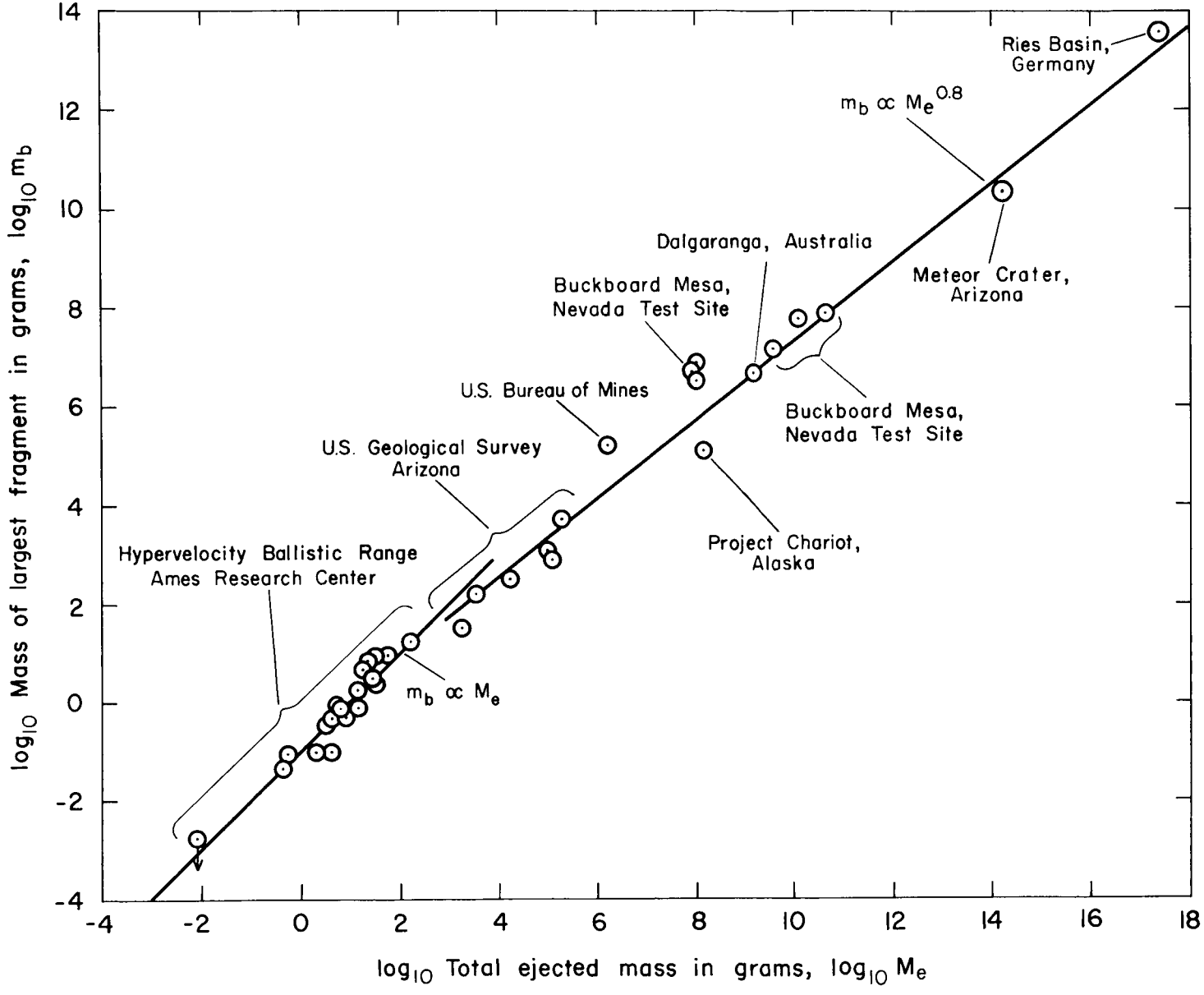

Figure 5.- Correlation of the mass of the largest fragment with total ejected mass for explosive and impact cratering events.

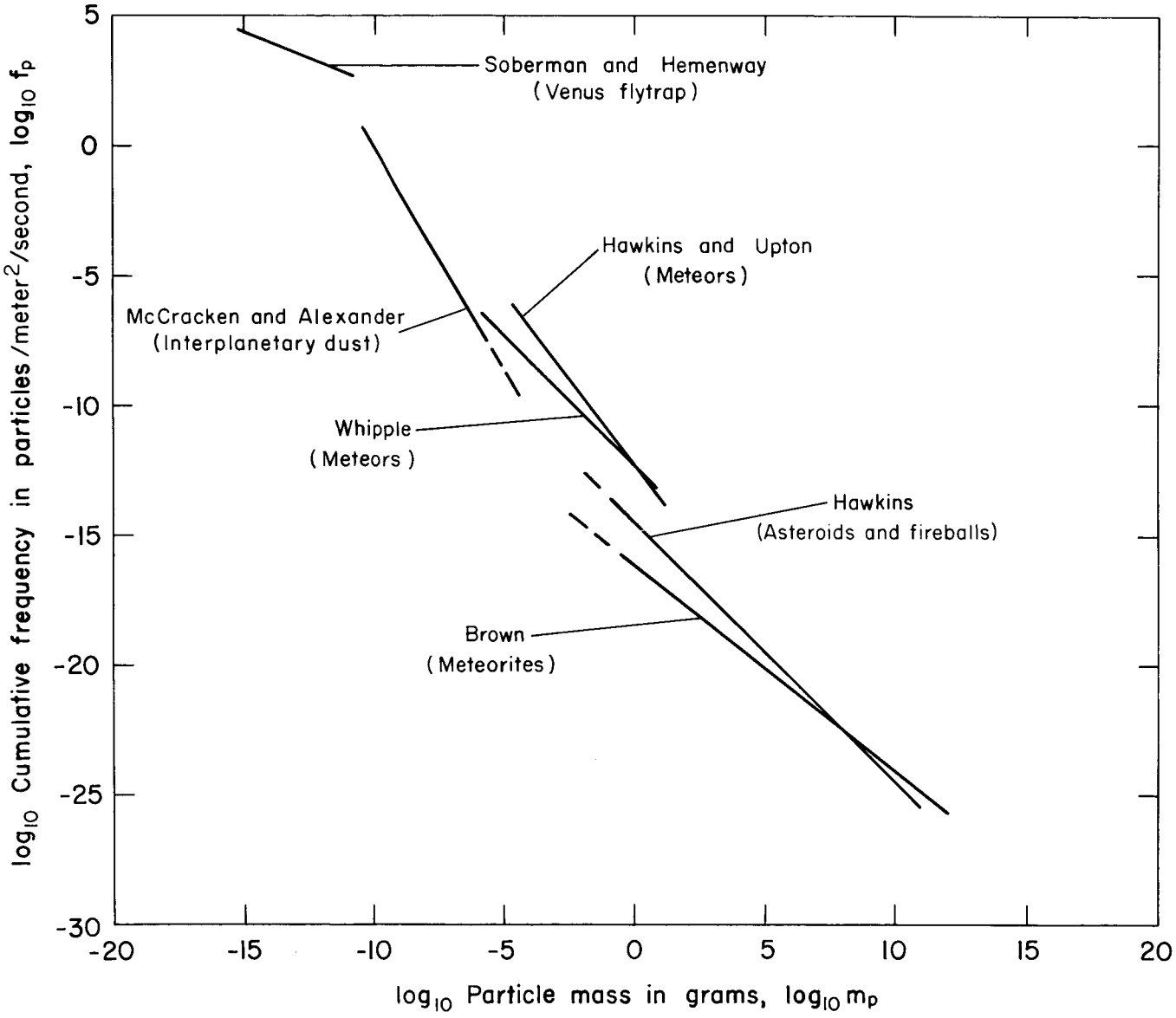

Figure 6.- Cumulative frequency-mass distributions for interplanetary debris.

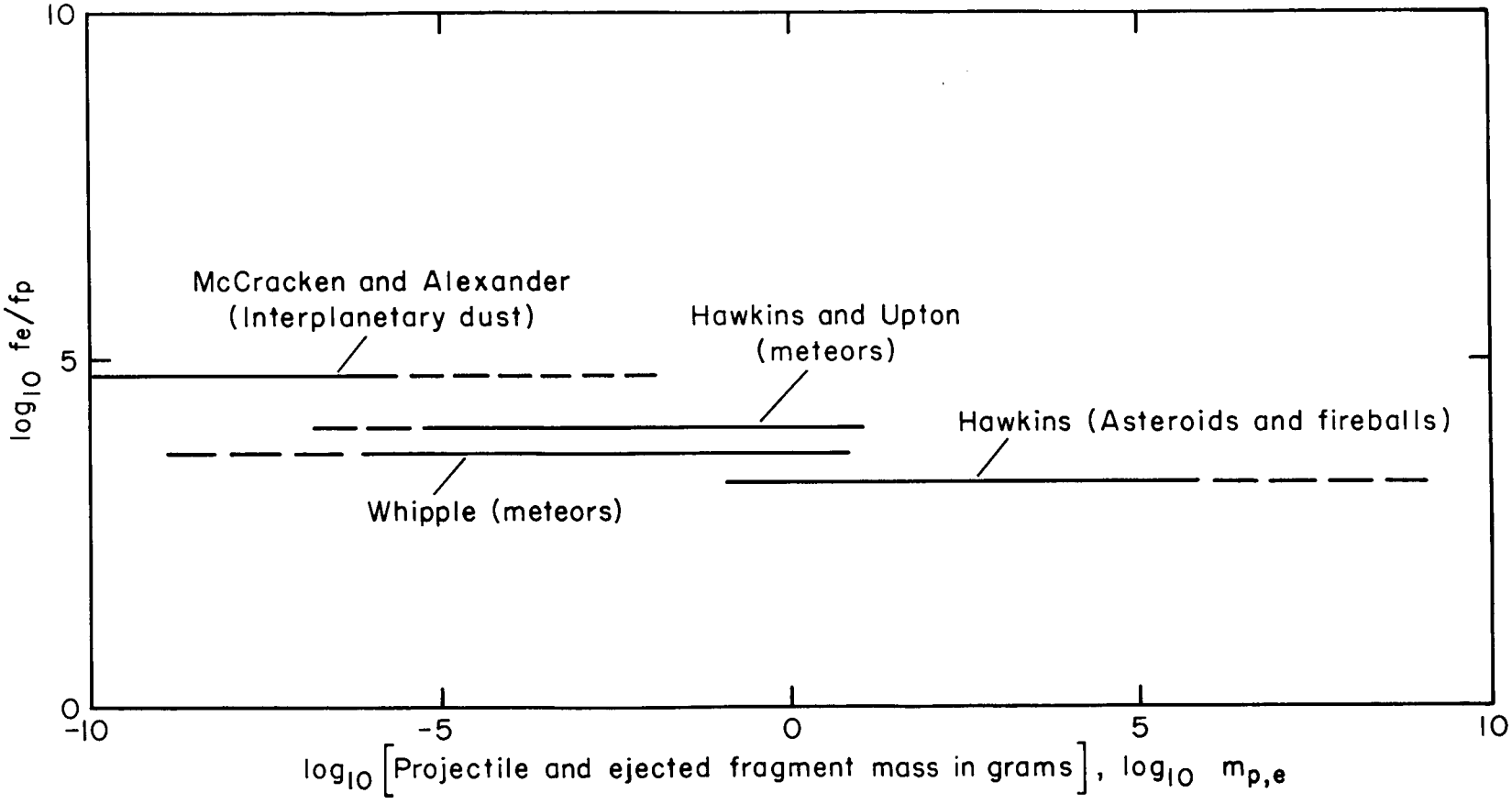

Figure 7.- The ratio of f_e/f_p for different types of projectiles.

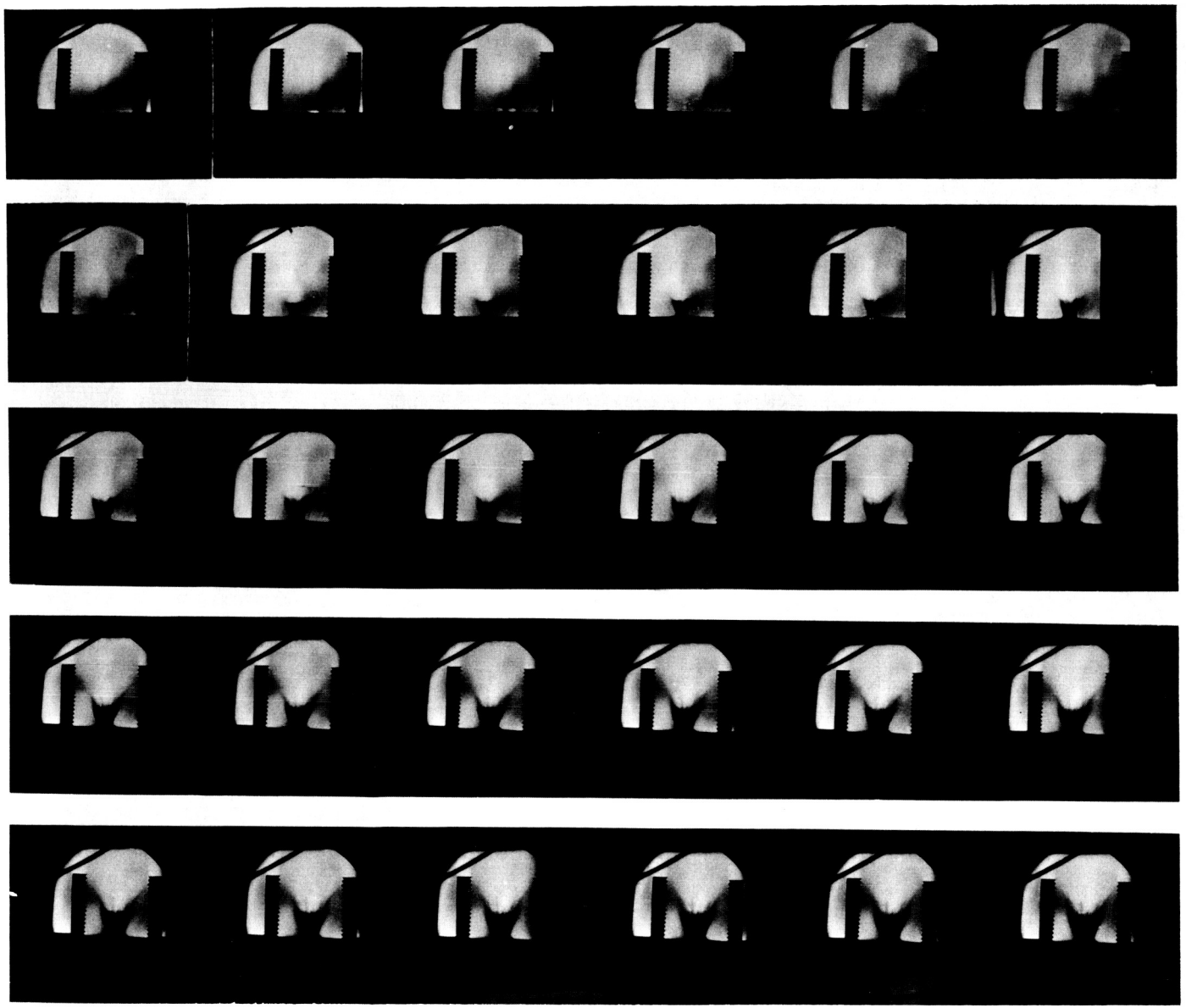

Figure 8.- High-speed framing camera records of an impact in basalt; framing rate = 1.04×10^6 frames per second; impact velocity = 6.4 kilometers per second.

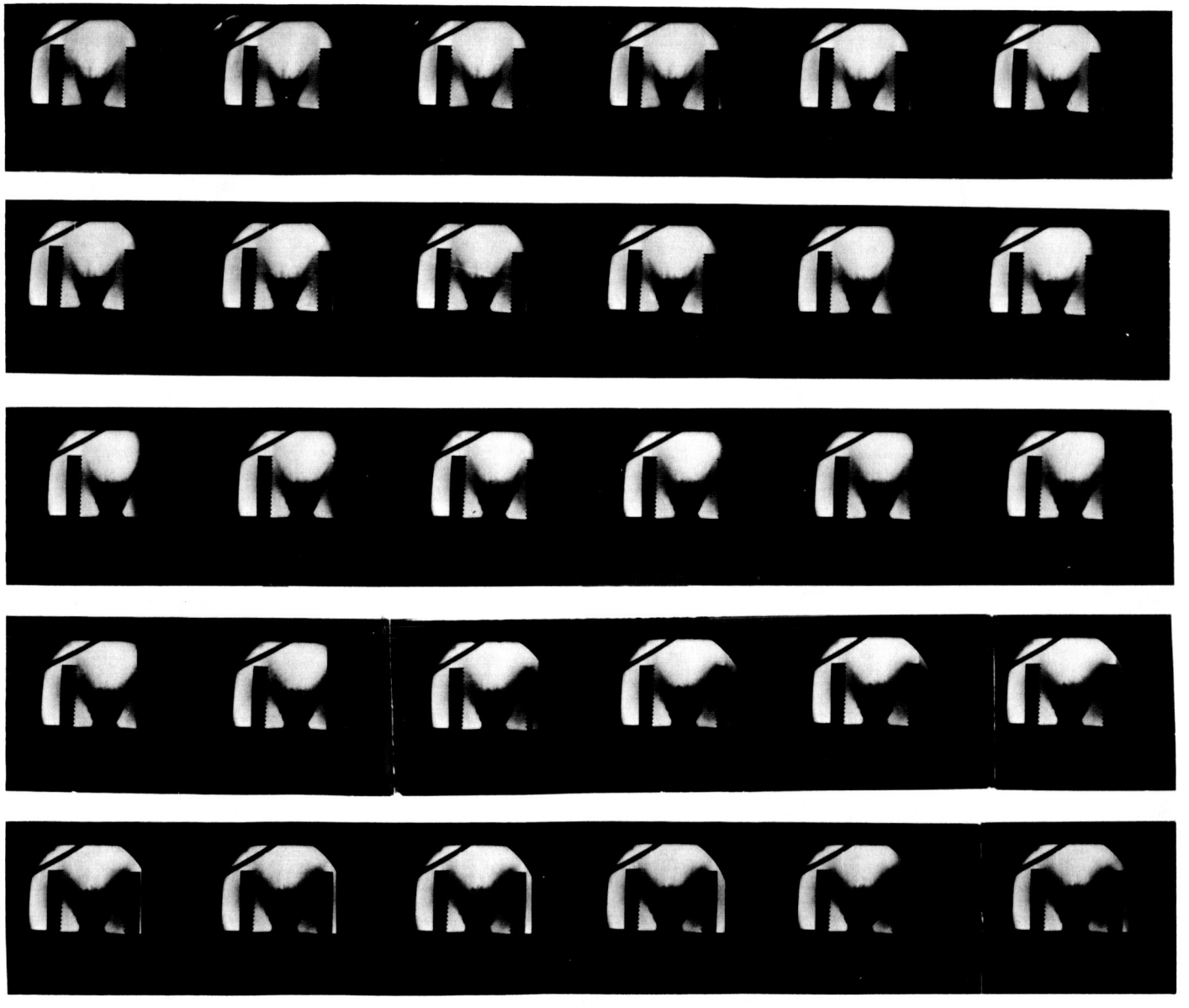

Figure 8.- High-speed framing camera records of an impact in basalt; framing rate = 1.04×10^6 frames per second; impact velocity = 6.4 kilometers per second - Continued.

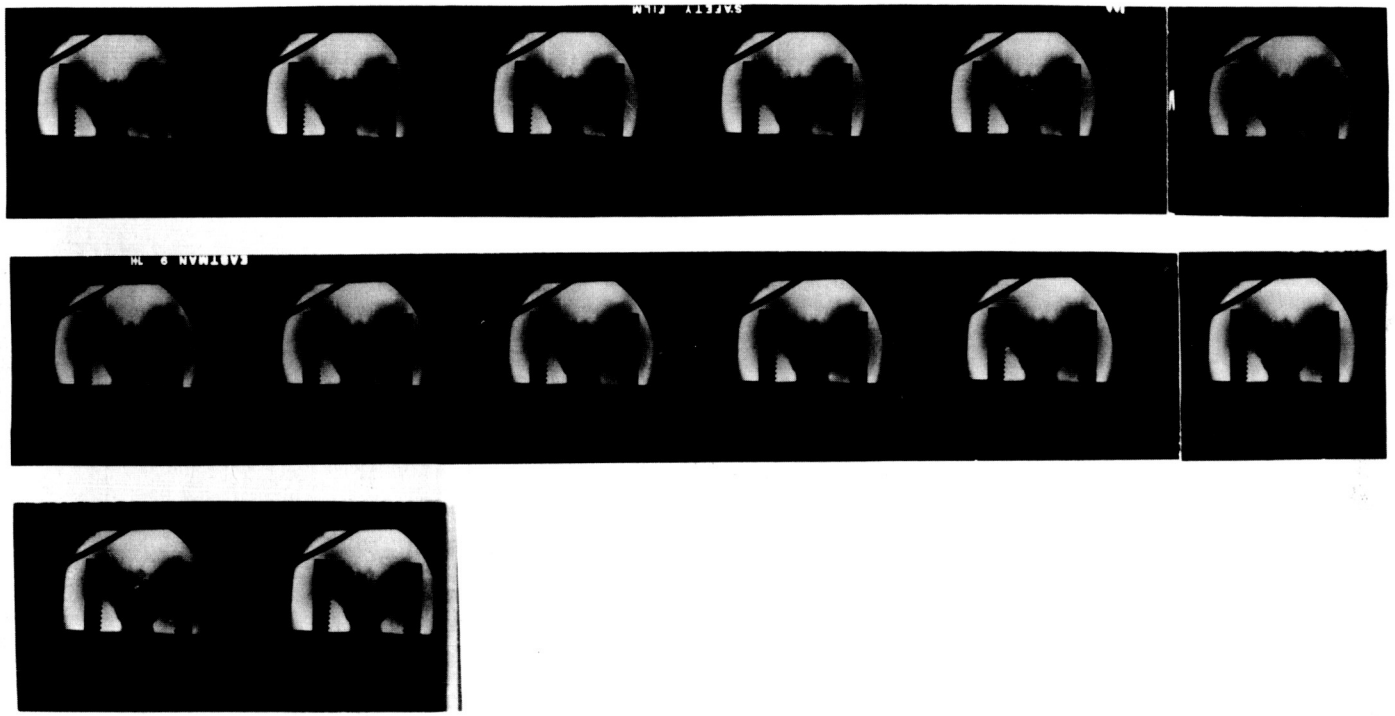

Figure 8.- High-speed framing camera records of an impact in basalt; framing rate = 1.04×10^6 frames per second; impact velocity = 6.4 kilometers per second - Concluded.

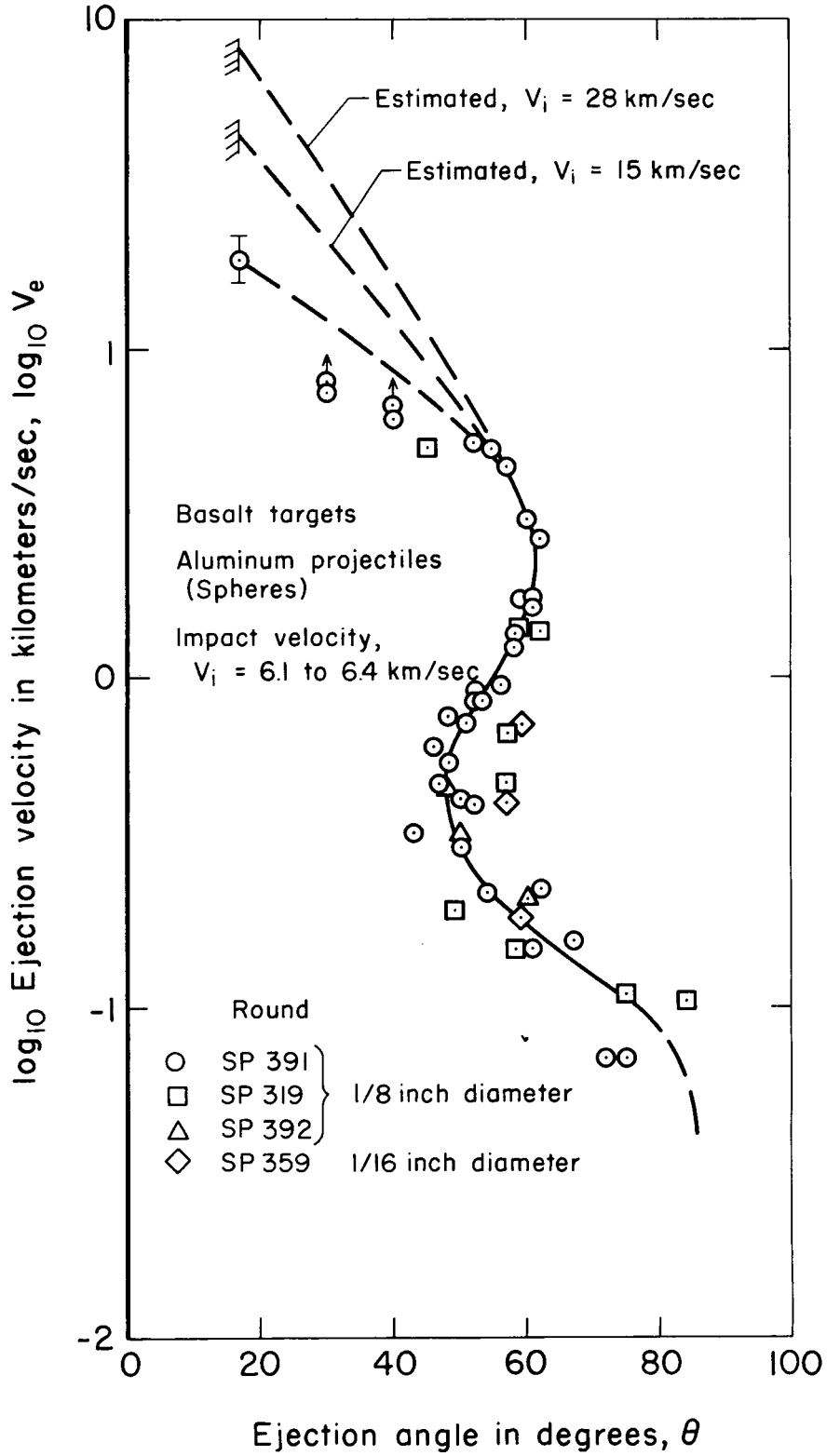

Figure 9.- Variation of ejection velocity with ejection angle for fragments thrown out of craters formed in basalt by hypervelocity impact.

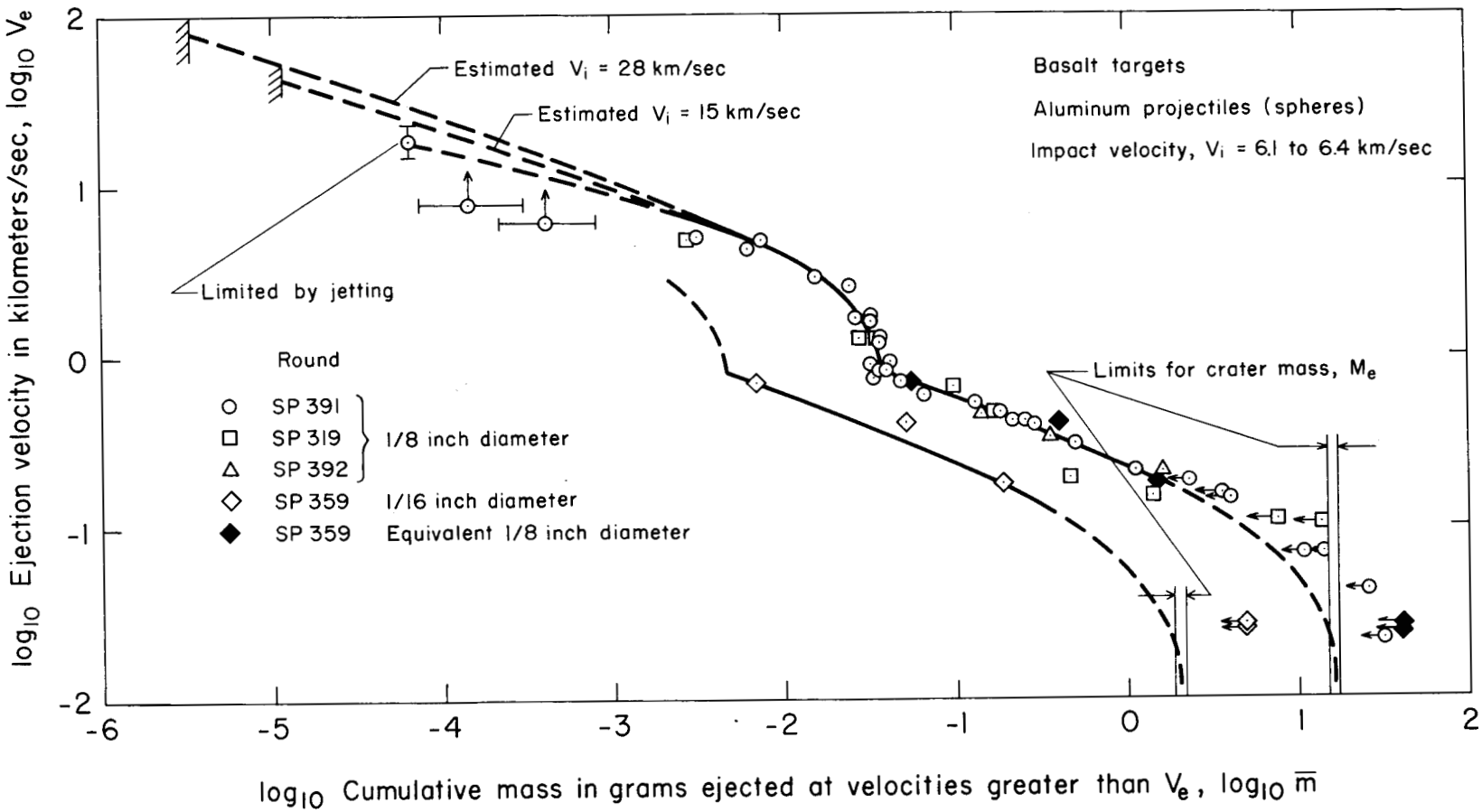

Figure 10.- Cumulative mass ejected in excess of a given velocity for fragments thrown out of craters formed in basalt by hypervelocity impact.

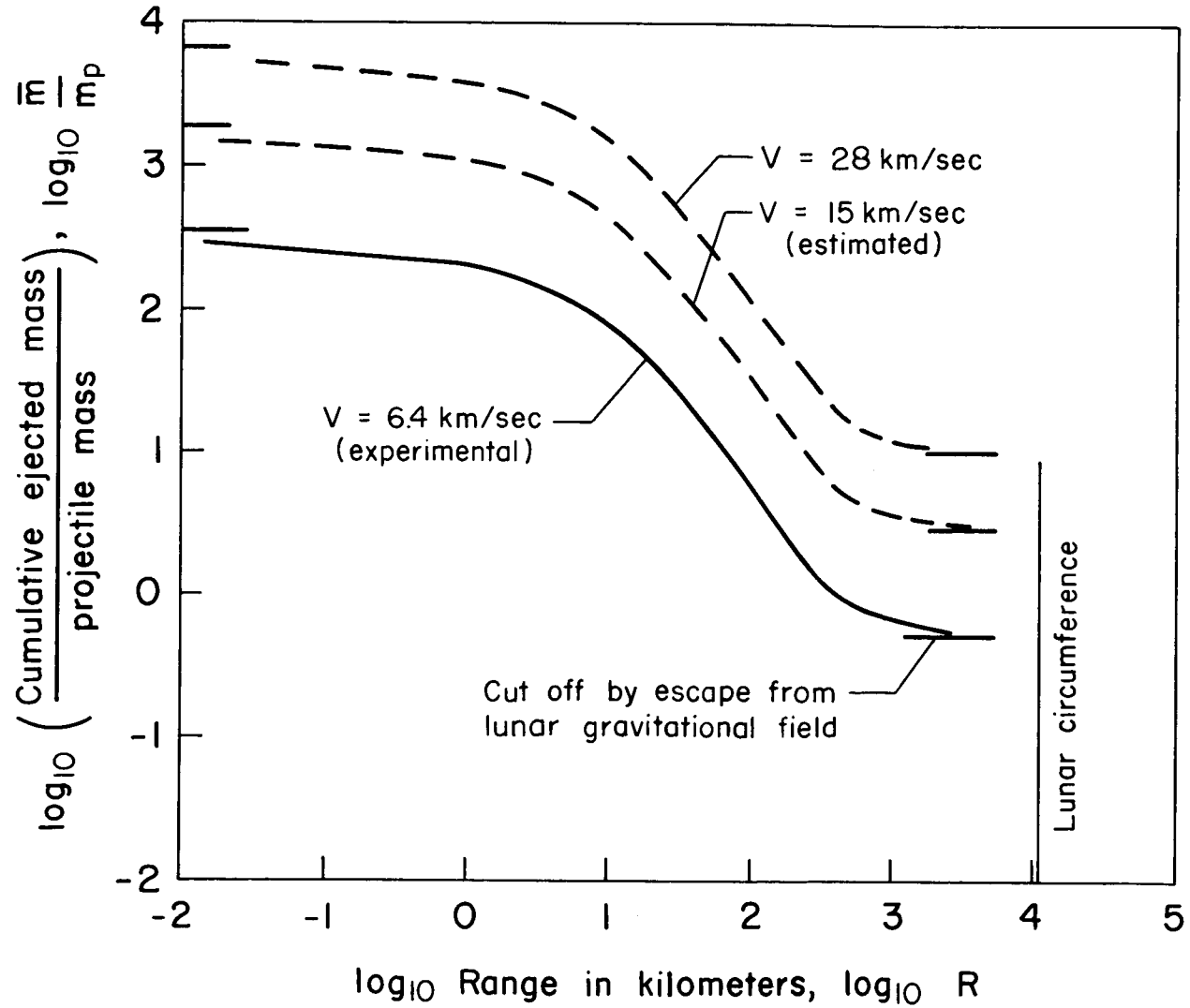

Figure 11.- Distribution across the lunar surface of the mass ejected from impact craters formed in basalt.

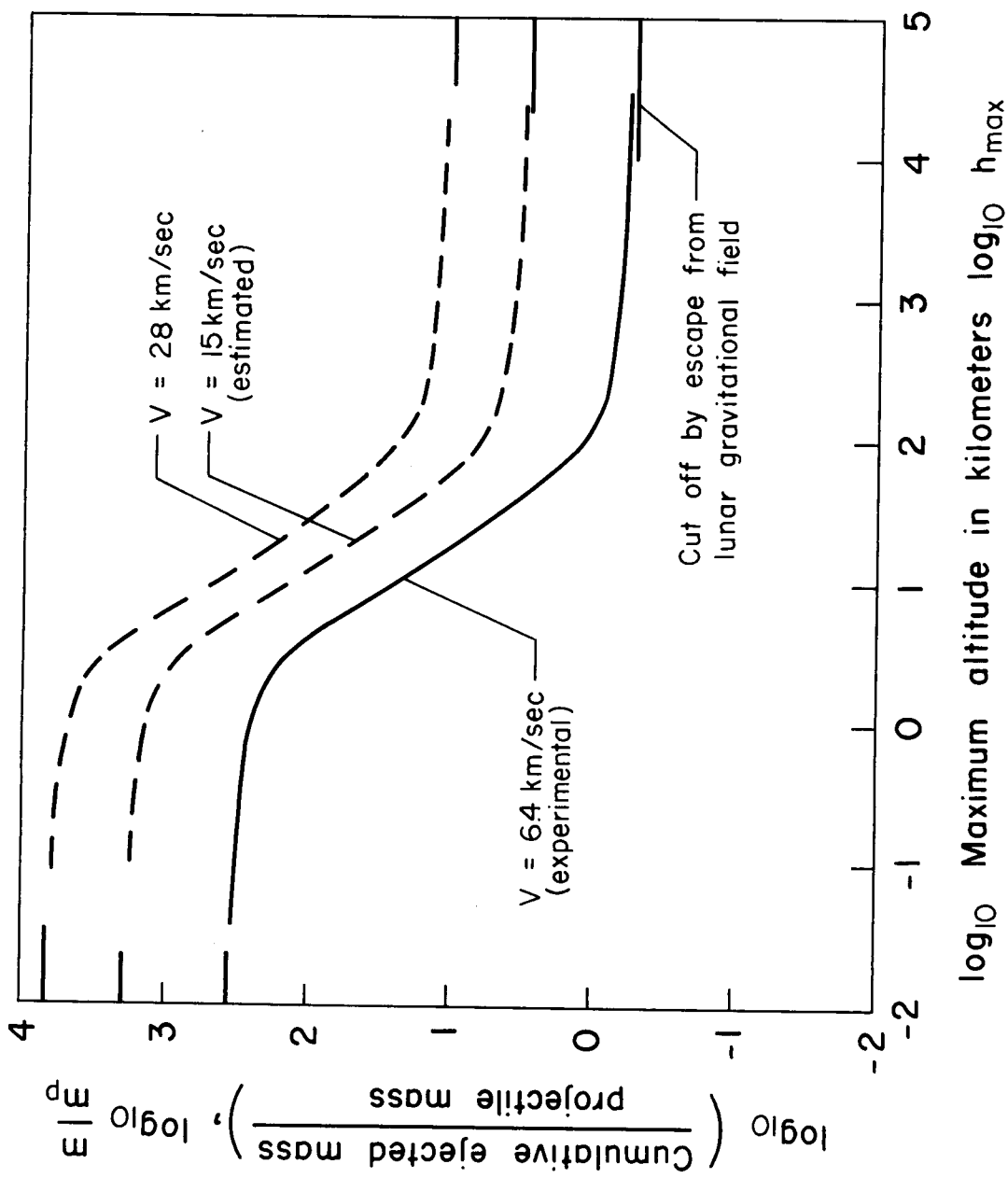

Figure 12.- Distribution above the lunar surface of the mass ejected from impact craters formed in basalt.